J. of Supercritical Fluids 164 (2020) 104892

Contents lists available at ScienceDirect

The Journal of Supercritical Fluids

journal homepage: www.elsevier.com/locate/supflu

Lansoprazole loading of polymers by supercritical carbon dioxide impregnation: Impacts of process parameters

Arezu Ameri[a,b], Gholamhossein Sodeifian[a,b,c,*], Seyed Ali Sajadian[a,b,d]

[a] Department of Chemical Engineering, Faculty of Engineering, University of Kashan, 87317-53153, Kashan, Iran
[b] Laboratory of Supercriritcal Fluids and Nanotechnology, University of Kashan, 87317-53153, Kashan, Iran
[c] Modeling and Simulation Centre, Faculty of Engineering, University of Kashan, 87317-53153, Kashan, Iran
[d] South Zagros Oil and Gas Production, National Iranian Oil Company, 7135717991, Shiraz, Iran

HIGHLIGHTS

- Lansoprazole was successfully impregnated onto PVP and HPMC for the first time.
- The effect of temperature, pressure impregnation and time was investigated.
- Impregnation process was optimized using BBD.
- Rise in temperature had the most effect on drug loading.
- The structure and behavior of drug and polymers were analyzed.

GRAPHICAL ABSTRACT

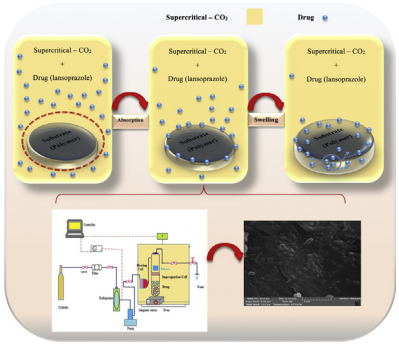

ARTICLE INFO

Article history:
Received 5 December 2019
Received in revised form 30 April 2020
Accepted 4 May 2020
Available online 12 May 2020

Keywords:
Lansoprazole
PVP
HPMC
Impregnation
Supercritical fluid (SCF)
Supercritical solvent impregnation (SSI)

ABSTRACT

This is the first work to load HPMC and PVP by the lansoprazole (LPZ) through supercritical solvent impregnation (SSI). The process was carried out at laboratory scale under various sets of conditions in terms of pressure (150–250 bar), temperature (308–328 K), and impregnation time (60–180 min). The results showed that an increase in any of the investigated parameters increased the drug loading, and that the temperature imposed the strongest effect on the drug loading. Moreover, impregnation loadings onto the PVP and HPMC were found to range from 0.56% to 0.61% and from 1.16% to 1.30%, respectively. For both polymers, the best results were obtained at a pressure of 250 bar and a temperature of 328 K with an impregnation time of 180 min. The processed drug was further investigated by XRD, SEM, DSC, FTIR, and DLS analyses. The final results indicated superior loading of the drug onto the HPMC rather than the PVP.

1. Introduction

Being among the most commonly used drugs for gastrointestinal disorders, the lansoprazole (LPZ) is available in various forms, including capsules, dispersible tablets, and enteric-coated suppositories. Chemically speaking, LPZ refers to 2-(2-benzimidazolysulfinylmethyl)-3methyl-4-(2,2,2-trifl-

* Corresponding author.
E-mail address: sodeifian@kashanu.ac.ir (G. Sodeifian).

https://doi.org/10.1016/j.supflu.2020.104892
0896-8446/

uoroethoxy) pyridine [1]. Thanks to its function as a gastric proton pump inhibitor (PPI), it has been applied as a prophylactic or therapeutic agent for the treatment of the gastritis disease, digestive ulcer, reflux esophagitis, upper gastrointestinal hemorrhage, gastric cancer, postoperative stress-resulted ulcer, and the illnesses associated with the helicobacter pylori [2–4].

Solubility is a significant factor that affects not only the drug design, but also its separation and purification procedures. As a methanol-soluble compound, the LPZ exhibits very low solubility in ethanol, relatively low solubility in ethyl acetate and acetonitrile, and just a little solubility in ether, with the compound being insoluble in hexane and water. Measurements have indicated a water-solubility of 0.044 mg/mL for this drug [2,5,6].

A common approach to increasing the solubility and bioavailability of a drug inside the human body is to reduce the drug particle size. There are several methods for synthesizing nano-sized particles, each of which leading to the preparation of nanoparticles with different properties. Recently, supercritical fluids (SCFs) have been proposed as suitable media for the production of micro- and nano-sized particles of drugs [7]. Common SCF processes have returned promising results; these include gas anti-solvent (GAS), rapid expansion of the supercritical solution (RESS), supercritical anti-solvent (SAS), particles from gas-saturated solution (PGSS), and solution-enhanced dispersion by supercritical fluids (SEDS) [8–11]. However, it is still difficult to control the characteristics of the particles produced through these processes, especially in the case of coprecipitation of active compounds together with carrier materials. As an alternative for obtaining a drug delivery system, impregnation in supercritical carbon dioxide can be used to incorporate the active compound into previously formed particles of the carrier material [10].

Among others, outstanding properties of the SCFs include liquid-range density, superior solvating power, low viscosity, and enhanced diffusivity and mass transfer coefficient, which make them good candidates for replacing the organic solvents in a large number of applications in the industrial context (*e.g.* chemical and biochemical reactions, separation and purification processes, and particle synthesis schedules) as well as more recent applications related to the processing of polymers and other materials [12–17]. The carbon dioxide offers numerous favorable properties, including moderate critical pressure and temperature (7.38 MPa and 304 K, respectively), non-toxicity, non-flammability, non-explosiveness and abundant availability at high levels of purity. Moreover, under ambient pressure and temperature conditions, CO_2 is gaseous and therefore its separation at the end of the process requires a depressurization stage. Besides, SC−CO_2 has biocidal properties [18–20]. Thanks to its unique characteristics, the carbon dioxide has been extensively used as a supercritical solvent in the chemical processes encountered in the pharmaceutical and biochemical industries where miniaturization of the drug particles is a preliminary objective for the ultimate goal of enhanced bioavailability of the drug in the body [21–28].

The supercritical solvent impregnation (SSI) has emerged as an effective method to incorporate active compounds into materials for different applications. In particular, SSI is an innovative technique to produce pharmaceutical composite systems [29–31]. Using this process, one can load the active compound onto existing carrier medium particles, making it simpler to control the characteristics of the ultimate product. This is because of the independence of the stages wherein the carrier medium particles are formed and then the active compound is loaded on the previously formed particles. Three methodologies have been developed for implementing the SSI process, namely static, semi-dynamic, and dynamic methods. The balance of interactions among the drug, impregnation support and the SCF make the drug molecules impregnate in the carrier medium; this ends up with the adsorption of the drug molecules, which herein refers to the physicochemical attachment of the drug molecules onto the polymeric matrix support [32]. When applied to polymers, the plasticizing effect (glass transition temperature depression) and the swelling effect of the SCF on glassy polymers can influence solute loading and impregnation [33]. Moreover, the SSI has been employed in several fields within the chemical and food industry. The most common cases include the bioactive impregnation, supercritical aerogel impregnation, porous scaffolds, polymer dyeing and drug-loaded implants [33–39].

Mining into the previously published literature showed that Rojas et al. [31] investigated supercritical impregnation for food applications and reviewed the investigated impregnation parameters. In addition, the effects of the processing variables of the SSI process (pressure, temperature, depressurization rate and time) were discussed in terms of the incorporation of active compounds into polymer structures.

Bouledjouidja et al. [40] investigated the application of SC−CO_2 to impregnate ciprofloxacin (CIP) and dexamethasone 21-phosphate disodium (DXP) in intraocular lenses (IOLs). Optimal operating conditions for P-HEMA IOLs were determined by investigating different parameters including the temperature, pressure, the rate of pressure changes, cosolvent application, and the impregnation time. In all cases, the DXP exhibited further impregnation in P-HEMA, as compared to the CIP. In another work, the authors studied several drug components and IOLs combinations and demonstrated that an effective and in-depth impregnation is influenced by different parameters including the temperature, pressure, the rate of pressure changes, cosolvent application, and the impregnation time. In all cases, the sustained release was observed while preserving the optical properties of the IOLs [41–43].

Costa et al. [44] sought to improve particular eye diseases. They used the SCF impregnation method, considered the optimal experimental conditions (T =40 °C, P = 170 bar, t_i =90 min), and impregnated the commercially available silicon-based hydrogel contact lenses (Balafilcon A) using a pair of anti-glaucoma drugs, namely acetazolamide and timolol maleate. Results showed that the drug-loaded contact lenses could not only treat the eye disease, but also mitigate the unwanted side effects.

Examining the SC impregnation of food packaging films for the purpose of improved antioxidant characteristics, Bastante et al. [45] suggested that, unlike other approaches to the preparation of antioxidant films, the SSI provides a film with antioxidant capability immediately upon the manufacturing, making the final product solvent-free. Tang et al. [46] employed the SC impregnation to load the ibuprofen onto already prepared chitosan film. Investigating the contributions from the pressure and temperature into the morphology of the chitosan film upon loading the ibuprofen, an improvement in the drug loading capacity (DLC) was observed in comparison to similar methods, with DLC increasing from 7.9 to 130.4% during this process. In addition, the drug release could be controlled to minimize the precipitation. Bouledjouidja et al. [47] applied two processes, namely incipient wetness and SC impregnation, to load fenofibrate, a slightly water-soluble drug, into silica samples with an ordered mesoporous structure. The results indicated superior yield of the latter method within shorter processing times. In another study, Belizón et al. [38] conducted a study where antioxidant mango polyphenols were SC-impregnated into a food-grade multilayer PET/PP film to achieve enhanced food packaging for the ultimate goal of increasing the product shelf life while maintaining its flavor and safety requirements. Varona et al. [10] presented a research on the production of natural pesticides, instead of chemicals, to make the essential oil a sort of efficient additive for the livestock farming industry. The essential oil from lavandin was further impregnated into modified starch using the SC impregnation method. The results showed higher loading per-

Table 1
Review of some published works on the subject-matter of impregnation in various contexts (*e.g.* the food and pharmaceutical industries).

Compound	Method	Cosolvent	Material	Pressure (MPa)	Temperature (°C)	Depressurization rate (MPa/min)	Time (h)	Highest impregnation percentage (wt/wt)%	References
Ketoprofene	Semi static	–	PVP(polyvinyl pyrrolidone)	19	40 to 60	-	120	58	[52]
Flurbiprofen	Semi static	–	P(MMA-EHA-EGDMA)	10 to 18	35 to 40	-	3 and 5	0.82	[53]
α-tocopheryl acetate	Semi static	–	Silica mesoporous	8 to 15	40	-	1	53	[54]
Roxythromycin	Static	–	PLLA films	8 to 30	40 to 70	in 10 minutes	0.5 to 2	10.5	[55]
Lavandin oil	Static	–	Modified starch powder	10, 11 and 12	40 to 50	0.07 to 0.15	2	15	[10]
Lactulose	Static and dynamic	Ethanol:water	Chitosan scaffolds and microspheres	10	100	0.6, 1 and 3.3	1 and 3	8.6	[56]
Lecithin and erythorbate	Static	Ethanol	HDPE, high-density polyethylene films	20.7	65	-	0.75	-	[57]
Flax oil	Static and dynamic	Ethanol	b-glucan aerogels	15 and 30	40 and 60	-	2, 6 and 8	65.39	[58]
Indomethacin	Static	–	PLA/PLGA	18	40	6 to 0.2	1	-	[59]
Oregano Essential oil	Static	–	Starch microspheres	8 to 15	40 to 50	0.0083 to 0.11	3, 6 and 24	-	[60]
Natamycin	Static	Ethanol	Alginate films	20	40	-	2.5, 4 and 14	16.29	[61]
Thymol	Static	–	LLDPE films	7, 9 and 12	40	-	4	1.3	[62]
Cinnamaldehyde	Static	–	Cassava starch films	15 and 25	35	1 and 10	3 and 15	0.25	[63]
Ketoprofen	Static	–	PLLA, PET and PP films	10 to 35	40 to 140	0.0017, 0.1 and 0.06	3	32.5	[64]
Aspirin	Static	–						8.1	
Indomethacin	Static	Ethanol–water	PVP and Soluplus	10 and 15	60 and 70	in 30 s	2	-	[65]
2-nonanone	Static	–	LLDPE films	12, 17 and 22	40	1 and 10	3	0.34	[66]
Thymol	Static	–	Starch gels	15.5	35	0.3	24	4.02	[67]
Thymol	Static	–	Cellulose acetate films	10, 15 and 20	35 and 50	0.3	2 to 32	72.26	[68]
Vitamin K3 and D3	Static	–	Alginate aerogel spheres	15 and 20	40	0.3	1 to 24	~12	[36]
Vitamin D3	Static	–	Alginate aerogel spheres	8	5, 15, 25 and 35	-	1 to 24	~12	[22]
Eugenol	Static	Ethanol	LLDPE films	10, 12 and 15	45	0.5, 1 and 1.5	24	6	[69]
Phytol	Static	–	Silica and alginate aerogels	200	40	0.2	28 and 32	30.1	[70]
Thymol	Static	–	Cellulose acetate films	10	35	-	2 and 5	63.84	[71]

Table 1 (*Continued*)

Compound	Method	Cosolvent	Material	Pressure (MPa)	Temperature (°C)	Depressurization rate (MPa/min)	Time (h)	Highest impregnation percentage (wt/wt)%	References
Phytosterols	Semi Static	–	Nanoporous starch aerogels	45	70	1 L/min (atmospheric conditions)	3	5.5	[72]
CIP	Static	Ethanol	P-HEMA	8 to 20	35	0.2	0.5 to 4	0.41	[40]
DXP	Static	Ethanol		8 to 20	35	0.2	2	1.45	
Olive leaf extract and caffeic acid	Static	Ethanol	PET/PP films	10, 20, 30 and 40	35 and 55	0.1 and 10	0 to 4	-	[73]
Clove essential oil	Static	–	LLDPE films	12 and 20	25, 35 and 45	-	3	4.02	[16]
Phytosterols	Semi dynamic	–	Nanoporous starch aerogels	45	70, 90 and 120	1 L/min (atmospheric conditions)	4	9.9	[35]
Thmoquinone and R-(+)-pulegone	Static	–	LDPE films	10 and 15	45	0.5 and 2	2 and 4	5.59	[74]
Compound	Method	Cosolvent	Material	Pressure (MPa)	Temperature (°C)	Depressurization Rate (MPa/min)	Time (h)	Highest impregnation percentage (wt/wt)%	References
Thmoquinone and R-(+)-pulegone	Static	–	LDPE/Sepiolite nanocomposite films	9 and 13	45	0.5 and 2	2 and 4	8.6	[75]
Thymol	Static	–	LDPE/C20A	12	40	1 and 10	0.25 to 5	1.19	[76]
Cinnamaldehyde	Static	–	PLA films	9 and 12	40	0.1 to 10	3	13	[77]
Thymol	Static	–	PLA films	9 and 12	40	0.1 to 1	3	20.5	[78]
MLE(mango leaf extract)	Static	Methanol and ethanol	Polyester Tissue	40 and 50	35 and 55	0.06, 0.11 and 2.5	22	55.8	[79]
Thymol	Static	–	PLA/nanofibers	12	40	1	22	24	[78]
ZnO/NiO nanocomposite	Static	Methanol	Ordered mesoporous Alumina	20	50	-	4	10.33	[80]
Cinnamaldehyde	Static	–	PLA electrospun mats	12	40	1	3	3.29	[81]
Methyle gallat	Static	Ethanol	PET/PP films	10 and 20	35, 45 and 55	0.2	3, 15 and 22	0.004	[38]
Thymol	Static	–	LDPE/Cloisite 20A nanocomposite films	9, 12 and 15	40	10	0.5 to 5	1.62	[78]
Carvedilol	Static	–	PVP, HPMC, Soluplus and Eudragit	30	100	1.5	2	-	[82]
Thymol	Static	–	PLA	20 to 30	100 to 120	0.05	2 and 24	19.8	
Thymol	Dynamic	–	PLA	30	100	0.064 ± 0.017	2 to 5	1.1 ± 0.019	[83]
Thymol extract	Semi Static	–	PLA	30	100	0.064 ± 0.17	2 to 5	0.7 ± 0.07	
Hydromorphone	Static	–	PLGA microparticles	14	40	-	0.5 to 1	9.2	[26]
Carvacrol	Static	–	Cellulose acetate	21	50	0.3 to 36	0.5 to 2	31.4	[84]
Carvone	Static	–	LDPE films	7.6 to 9.7	35 and 60	0.6	2 to 4	4.8	[85]

Table 1 (*Continued*)

Compound	Method	Cosolvent	Material	Pressure (MPa)	Temperature (°C)	Depressurization rate (MPa/min)	Time (h)	Highest impregnation percentage (wt/wt)%	References
Eugenol	Static	Ethanol	Polyamid fiber	8 to 12	60	0.5 to 5	2	15	[86]
Nimesulide	Static	–	Polycaprolactone	10 to 20	35, 40, 50 and 60	1	4 and 8	35	[87]
Eutectic blend (LA:MA)	Static	–	Gauze	10	40	in 1 minute	1	-	[88]
Lycopene	Static	–	Hydrolysed Collagen (LLHC)	15 and 25	50 and 60	in 15 minutes	0.75	8.5	[89]
Nitrendipine	Static	Ethanol	PLLA-PEG-PLLA	10 to 20	35, 45 and 55	-	2	10.5	[90]
Caffeine	Static	–	MG-MOF-74	10	40	2	2 to 24	34.3	[91]
Caffeine	Static	–	MIL-53(Al)	10	40	2	2 to 24	32.1	
Carvacrol	Static	–	MG-MOF-74	10	40	2	2 to 24	30.1	
Carvacrol	Static	–	MIL-53(Al)	10	40	2	2 to 24	34	
α-tocopheryl(TOC)	Static	–	PP, PET and PP/PET	17	40	0.1	2 to 48	3.2 mg TOC/cm^2 film	[92]
Tetraethoxysilane(TEOS)	Static	–	Celgard membrane	30 to 43	40	-	24	-	[93]
Cinnamaldehyde	Static	–	PLA	12	40	1	-	11	[94]
Cinnamaldehyde	Static	–	PLA/C30B	12	40	1	-	12	
Thymol	Static	–	PLA	12	40	1	-	16	
Thymol	Static	–	PLA/C30B	12	40	1	-	17	
					Temperature (°C)	Depressurization rate (MPa/min)	Time (h)	Highest impregnation percentage (wt/wt)%	References
Acetazolamide	Static	Ethanol and water	Silica-based hydrogels	17	40	0.06	1.30	1.97	[44]
α-tocopheryl	Static	–	Ultra-high molecular weight PE	10–30	130–170	–	–	1	[95]
Acetazolamide	Static	Ethanol and water	Silica-based hydrogels	15–20	40–50	0.06	1,2 and 3	1.97	[96]
Ketoprofen	Static	–	PLGA	6.5–30	25–55	–	–	57	
Timolol maleate	Static	Ethanol and water	Silica-based hydrogels	17	40	–	–	1.8	[44]
Ibuprofen	Static	–	PVP	10	40	–	–	30	[50]
Piroxam	Static	–	PVP	10–60	40	–	–	3.9	[97]
Tranilast	Static	Ethanol	PLLA	22	80–120	–	–	0.9	[98]
Acetylsalicylic acid	Static	–	PLLA	8–10	40	2–30 mL/min	3	29	[99]
Triflusal	Static	–	PMMA	15–20	35–40	0.2–0.4	12–16	21.7	[100]
Ibuprofen	Static	–	PMMA	13.8–20.7	40–50	–	–	25	[15]
Cefuroxime sodium	Static	Ethanol	PMMA	8–20	35–60	–	1–5	0.063	[101]
Megesterol acetate	Static	–	PVP	13	40	–	–	0.08	[102]
Nimesulide	Static	–	PVP	16–19	45	–	–	9.7	[102]
Ppaclitaxel	Static	Ethanol	P(D.L)LA	20	40	–	3–5	0.13	[103]
Acetylsalicylic acid	Static	–	PP	10–35	40–130	–	3	5	[64]
Progesterone	Static	–	PU	15.2	45	–	–	8	[104]
Hydroxycoumarin	Static	–	PU	15	40	–	–	0.3	[105]

formance through the SC impregnation method, as compared to similar approaches including PGSS. Being a highly crystalline and slightly water-soluble drug, the indomethacin has been used for the treatment of ankylosing spondylitis, rheumatoid arthritis, acute gout disease, and osteoarthritis [48–50]. Gnog et al. [51] used a SCI method wherein chitosan was utilized as a polymer to enhance the indomethacin solubility through extending its surface area or making the drug stabilized. Table 1 presents a comprehensive review of the previously published works on the subject-matter of impregnation in various contexts (*e.g.* the food and pharmaceutical industries).

The two polymers used in this work, namely hydroxypropyl methylcellulose (HPMC) and poly(*N*-vinyl-2-pyrrolidone) (PVP), offered the following advantages when utilized as a coating material: (1) controlling the release mechanism and pattern as well as mechanical characteristics of the drug, (2) enhancing the formation and storage stability of the film, and (3) presenting potentials for developing site-specific drug delivery systems by which the gastrointestinal tract could be treated [106–111]. The HPMC is a natural polymer material that is mainly derived from cellulose as raw material [4]. It is a water-soluble compound exhibiting pH stability and significant thickening and adhesion properties. Possessing an amide ring, the poly(*N*-vinyl-2-pyrrolidone) (PVP) is a polar molecule, making it suitable for hydrogen bonding. It is soluble in water and many other polar solvents. The main features of the PVP include (1) a wide range of solubilities and solvent-compatibilities, (2) physiological neutrality, and (3) ability to form films and complexes with other materials.

Our investigations showed no previous report on the impregnation of HPMC and PVP polymers with LPZ drug by SSI. Therefore, the present study discusses the application of impregnation of drugs onto the polymers for improving the drug solubility in the body. For this purpose, the effects of three important parameters, namely temperature, impregnation time, and pressure, on the impregnation process were examined. Additionally, the structure and behavior of the impregnated drug nanoparticles were analyzed through scanning electron microscopy (SEM), dynamic light scanning (DLS), differential scanning calorimetry (DSC), X-ray diffraction (XRD) analysis, and Fourier transform infrared (FTIR) spectroscopy.

2. Material and methods

2.1. Materials

Lansoprazole (LPZ) (CAS no. 103577-45-3) with a minimum purity of 99% was provided by Amin Pharmaceutical Company (Isfahan, Iran). Fadak Company (Kashan, Iran) served as the provider of carbon dioxide (CO_2) (CAS No. 124-38-9) at a purity beyond 99.99%. These two materials were used as received with no further purification. The PVP, with an average molecular weight of $M_w \sim 40{,}000$ g/mole, and HPMC, with a viscosity of 4000 cPs (HPMC K4M), were procured from Sigma Aldrich (Germany). For each experiment, 100 mg of the powdered polymer, in pure form, was compacted (with no additives) in a hydraulic tablet press (Perkin Elmer, Hydraulische Presse) under a load of 10 tons to change the powder to a tablet with a diameter of 5 mm. The chemical structures of PVP, LPZ and HPMC are presented in Fig.1.

2.2. Methods

2.2.1. Design of experiment

Design of experiments (DOE) is a quality-focused approach that facilitates the process of product design and manufacturing. Using this method, the researcher can develop the whole production process by designing sub-processes that are resilient to environmental factors [112]. Among others, this methodology provides for examining the impacts of different variables on the response and modeling the relationships among them to identify the most significant input parameters affecting the output [113]. Various approaches to the DOE have been presented. As a common DOE technique, the three-level Box-Behnken design (BBD) has been employed to optimize the process parameters for LPZ-impregnated PVP and HPMC through SC-CO_2. In this work, the BBD was applied to study not only the main effects of pressure (150−250 bar), temperature (308.2–328.2 K), and impregnation time (60−180 min), but also their interaction effects and quadratic impacts on the drug loading. For this purpose, as shown in Table 2, the considered variables were designated as pressure (X_1), temperature (X_2), and time (X_3) and examined at three levels coded as -1, 0, and 1, indicating high, intermediate and low values, respectively. For the sake of statistical calculations, the relationship between the coded and actual values was described as follows:

Table 2
Uncoded and coded levels of independent variables used in the BBD for impregnation of LPZ/PVP and LPZ/HPMC.

Coded levels	Pressure (X_1, bar)	Temperature (X_2, K)	Time (X_3, min)
−1	150	308	60
0	200	318	120
+1	250	328	180

$$X_i = \frac{Z_i - Z_o}{\Delta Z} \tag{1}$$

where X_i is the coded value of the respective variable, Z_i is the actual value corresponding to the X_i, and Z_0 denotes the actual value at the center point. Accordingly, ΔZ expresses the step change of the considered variable.

The three variables were mathematically modelled using a quadratic polynomial model whose coefficients were calculated through a multiple regression analysis. The general form of this model is as follows:

$$Y = A_0 + \sum_{i=1}^{3} A_i x_i + \sum_{i=1}^{3} A_{ii} x_i^2 + \sum_{i=1}^{3}\sum_{j>1}^{3} A_{ij} x_i x_j + \varepsilon \tag{2}$$

where Y represents the predicted response, A_o is a constant coefficient, A_i is the first-order linear coefficient, A_{ii} is the quadratic coefficient, A_{ij} is the coefficient of interaction, x_i and x_j are coded levels of the respective independent variable, and ε is the associated random error [114]. Statistical analysis was performed using Design-Expert software (version 7.0.0). Analysis of variance (ANOVA) provides a summary of the considered parameters, their effects on the dependent variable, and the significance of their effects (p-value and F-value) [115,116]. The so-called adjusted coefficient of determination, R^2 adj., was used to evaluate the goodness-of-fit of the regression model. Finally, response surfaces were drawn in a 3D space to determine the optimum set of conditions for loading.

2.2.2. Supercritical carbon dioxide impregnation experiments

The SC-CO_2 impregnation tests were performed at lab scale, as schematically demonstrated in Fig. 2. The batch apparatus used in this work was made up of a CO_2 cylinder, a filter (Hylok, 6000 psi), a refrigerator, a high-pressure liquid CO_2 pump (Haskel pump, MSHP-110), a heating coil, an impregnation cell containing the polymers and the drug, an oven (AE−60), a magnetic stirrer, a vent, and a controller. Pressure measurements (WIKA) were performed at an accuracy of ±1 bar. In order to maintain the temperature at the desired level, the equilibrium cell was mounted in an oven (Froilabo model, AE−60, France) wherein the temperature mea-

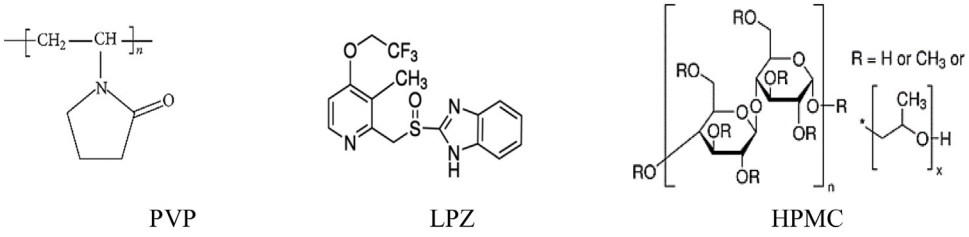

Fig. 1. Chemical structures of PVP, LPZ and HPMC.

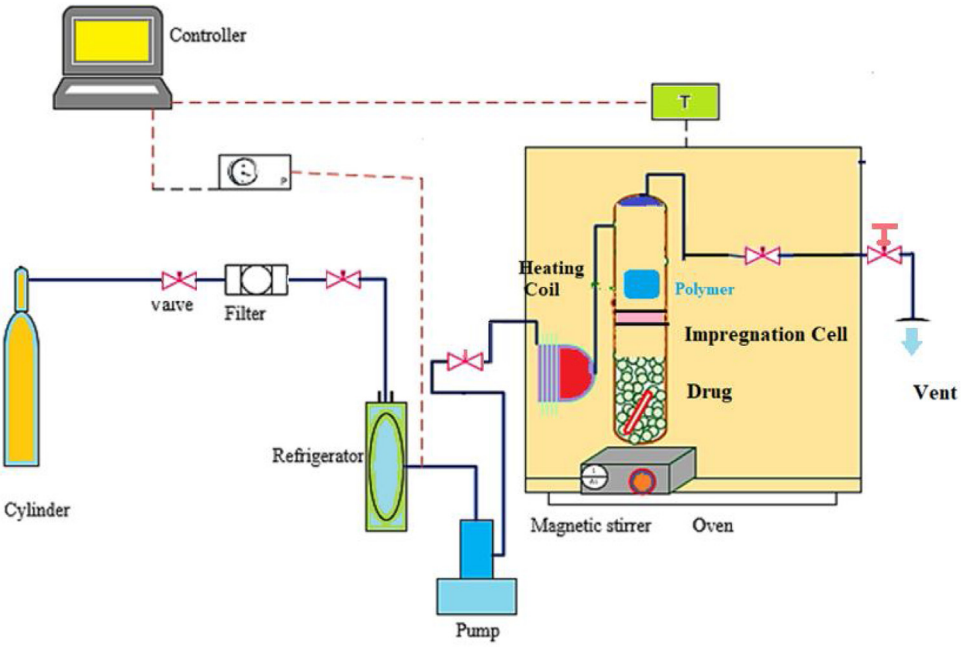

Fig. 2. Experimental apparatus of supercritical CO_2 impregnation.

surements were conducted at an accuracy of ±0.1 K. The cell was further equipped with poly-modulus PT100 sensors with a digital screen indicating the set and actual temperatures. At each run, 1000 ± 10 mg of LPZ was charged into the 100-ml static cell. The LPZ was situated in the bottom chamber of the cell, with the considered polymer tablet (100 mg) fitted in the upper chamber. In order to keep the undissolved LPZ inside the cell, the high-pressure equilibrium cell had its both sides sealed with stainless steel sintered disks (less than 1 μm). Furthermore, both polymers were separated inside the cell and covered with mesh filter bags (1 μm), and the same procedure was adopted to impregnate both of them.

In each test, firstly, the gaseous CO_2 was forced to pass through 1-μm pores of a filter before having it liquefied by reducing its temperature down to 273 K in the refrigerator unit. Next, the liquefied CO_2 at 60 bar (the pressure at the CO_2 storage tank) was subjected to pressurization using the reciprocating pump, with the pressure values recorded both from the pressure gauge and the pressure transducer. During this stage, the inlet valve was kept open until the desired temperature and pressure were reached. The active ingredient (LPZ) was thoroughly mixed with SC-CO_2 using a magnetic stirrer (200 rpm) and the LPZ-saturated SC-CO_2 was brought into contacted with the polymers for some static time, leading to swelling and impregnation of the polymers. Afterwards the cell was discharged at a constant pressure rate (5 bar/min, based on preliminary test) before removing the sample from the impregnation cell. In order to determine the drug loading, the LPZ content of the polymer was evaluated by UV–vis spectroscopy (UNICO-4802 UV–vis). For this purpose, 10 mg of impregnated polymer was introduced into a 5-mL container and then the container was filled with methanol. After the impregnation test, the sample was left at lab temperature for 3 h. Subsequently, for the sake of the spectrophotometry testing, the sample was sonicated for 10 min to ensure complete dissolution. The concentration of the LPZ in the solution was evaluated by absorbance measurements at 284 nm. Upon the absorbance measurements, the relationship between the LPZ concentration (C) and the absorbance (A) was expressed by a linear function. Stock solutions were sequentially diluted to obtain standard solutions. The standard solution was prepared in the concentration range of 5−100 μg/mL. The calibration equation obtained for the calibration curve of LPZ was A = 0.0086 C + 0.001 at a high regression coefficient (0.996). The following equation was used to evaluate the drug impregnation loading:

$$\text{Drug loading\%} = \frac{\text{amount of drug loading}}{\text{amount of polymers}} * 100 \quad (3)$$

Each experiment was performed in triplicate and average values of loading were reported as the final result.

2.2.3. Particle analysis

In this study, DLS, DSC, SEM, FTIR spectroscopy, and XRD analyses were utilized to determine the properties of the synthesized particles. The particle size distribution was studied using DLS analysis on a NANOPHOX particle sizer (Sympatec GmbH, Germany) equipped with a He-Ne laser producing 10-mW laser beams at a wavelength of 623 nm and operating at a scattering angle of 90°. To prepared the DLS samples, 10 mg of impregnated polymer was

introduced into a 5-mL container and then the container was filled with deionized water. The prepared samples were stirred for 1 h at lab temperature and then sonicated for 20 min to ensure complete dissolution before the DLS testing. The samples were further investigated in terms of thermal stability based on DSC analysis on a DSC 404 F3 Pegasus (NETZSCH, Germany). Here some 5 mg of each sample was heated from an initial temperature of 30 °C to a final temperature of 300 °C at a heating rate of 10 °C/min in an aluminum-made standard pan, with the samples subjected to an atmosphere of argon flowing at 10 mL/min. Morphology of the particles was characterized by SEM analysis on a VEGA 3 XMU apparatus (TESCAN, Czech Republic). For this purpose, the samples were sputter-coated with an alloy of gold and palladium using a SDC005 coater machine (BAL-TEC, Switzerland) at ambient temperature for 90 s. For the sake of FTIR analysis, a mixture of the sample (3 mg) and spectral-grade potassium bromide (KBr of 300 mg) was prepared using pestle and mortar. The mix was then pressed to obtain a KBr disk. The samples had their crystal structures examined using powder XRD analysis on a X′pert Pro MPD (PANalytical, Netherlands) based on Cu-Kα radiation (λ =0.154 nm) at room temperature in a 2Θ range of 10–80°. The Brunauer–Emmett–Teller (BET) analysis was conducted to evaluate the surface area of the sample by N_2 adsorption/desorption with an automated gas adsorption analyzer (BELSORP-mini II, Japan) at the boiling temperature of liquid nitrogen (−196 °C). Prior to the analysis, the samples were degassed under vacuum at 300 °C for 2 h. The nitrogen gas was injected into a sample and a reference chamber to calculate the relative pressures during the monolayer deposition on the sample. Finally, the specific surface area of the sample was measured on the BET plots considering the relative pressures.

3. Results and discussion

3.1. Optimization and validation of the model

Response surface methodology (RSM), and RSM-BBD in particular, refers to a well-known approach to DOE and optimal parametrization. As stated before, three variables were considered in this study, namely the pressure, the temperature, and the impregnation time. These were studied in certain ranges representing three levels (designated as −1, 0, and +1) to calculate optimal loading of LPZ/PVP and LPZ/HPMC. For this purpose, experiments were designed in a pressure range of 150–250 bar, a temperature range of 308–328 K, and an impregnation time range of 60–180 min. Table 3 reports the obtained values of the LPZ/PVP and LPZ/HPMC loading after the impregnation process upon performing a total of 17 experiments with the RSM-BBD. The results of ANOVA are tabulated in Tables 4 and 5, suggesting the best model out of the linear, two-factor interaction (2FI), and quadratic models. In this study, the quadratic model was applied for prediction and optimization of the impregnation loading. The last two columns of Tables 4 and 5 are important for specifying the parameters expressed in Tables 6 and 7. Based on the obtained *p*-values for LPZ/PVP (Table 4), the following parameters were found to impose significant effects on the yield of impregnation loading: temperature, time, pressure, pressure × time, time × time, and temperature × temperature. On the other hand, the temperature, pressure, time, pressure × time, and time × time imposed significant effects on the LPZ/HPMC loading.

Eqs. (4) and (5) are derived from the ANOVA results for the LPZ/PVP and LPZ/HPMC loadings, respectively:

$$\begin{aligned} LPZ/PVP\ Loading &= 0.83 + 0.18x_1 + 0.10x_2 + 0.076x_3 + 0.037x_1^2 \\ &- 0.036x_2^2 + 0.022x_3^2 - 0.010x_1x_2 + 0.017x_1x_3 \\ &+ 0.08x_2x_3 + Error \end{aligned} \quad (4)$$

$$\begin{aligned} LPZ/HPMC\ Loading &= 0.94 + 0.2x_1 + 0.12x_2 + 0.092x_3 + 0.023x_1^2 \\ &- 0.038x_2^2 + 0.028x_3^2 - 0.015x_1x_2 + 0.020x_1x_3 + 0.09x_2x_3 \\ &+ Error \end{aligned} \quad (5)$$

For the LPZ/PVP system, the coefficient of determination (R^2) and adjusted coefficient of determination (R^2 adj.) were calculated as 0.9929 and 0.9837, respectively, indicating a good agreement between the experimental data and predicted values of the response. For the LPZ/HPMC system, however, the R^2 and R^2 adj. were found to be 0.9920 and 0.9817, respectively, reflecting a divergence of less than 0.02. Upon changing the effective parameters, the drug loading on the PVP and HPMC changed in the ranges of 0.56–1.16% and 0.61–1.30%, respectively.

3.2. Effects of operating parameters on the loading of impregnated LPZ/HPMC and LPZ/PVP

A number of previous works have reported the use of SC impregnation of active pharmaceutical ingredients for controlling the release of active ingredients of drug products (see Table 1), where the effects of different parameters on the output have been analyzed. In this study, effects of temperature, pressure and impregnation time were examined on the impregnation process of LPZ on PVP and HPMC using SC-CO_2. Figs. 3a, b and c show 3D graphs of the obtained response surfaces for the LPZ/HPMC system, while Figs. 3d, e and f represent the same for the LPZ/PVP system.

3.2.1. Effect of temperature

The SSI process is a complex process governed by thermodynamic conditions and mass transfer phenomena between the involved components: the CO_2 as the carrier, the active ingredient, and the matrix. The solubility, the diffusivity and the affinity of the active ingredient with the matrix are known to affect the process, as does the thermodynamic behavior of the polymer (swelling and plasticizing effects) [38]. The temperature effects on sorption and diffusivity of CO_2 in polymers show opposite trends. Accordingly, with increasing the temperature, the sorption decreases while the diffusivity increases. The combined effect of sorption and diffusion can be seen by the permeability [117–120]. Generally speaking, with increasing the CO_2 sorption into polymers, one can tailor the polymer properties such a way to obtain a new morphology, *e.g.* desired pore size distribution. The greater the swelling, the quicker and more complete the impregnation-related diffusion [121,122]. The temperature can directly affect the solvating power and diffusivity of CO_2 and the thermodynamic behaviors of both the polymer (swelling and plasticizing effect) and the active ingredient. In general, the solubility of LPZ in CO_2 increases with temperature (above the crossover point) [123], positively affecting the impregnation of the active ingredient. In this work, the effect of temperature was evaluated in the range of 308–328 K. The LPZ impregnation into each polymer at different temperatures and a fixed pressure of 200 bar is presented in Figs. 3a and d. According to the figures, with increasing the temperature from 308 K to 328 K, the drug loading on the HPMC and PVP increased, positively contributing to the impregnation of the HPMC and PVP. The same increasing trend was observed at a pressure of 150 bar, although a decline in LPZ solubility was reported in our previous work [123]. Accordingly, a pressure of 210 bar was determined as the crossover pressure of LPZ, beyond which an increase in temperature negatively affected the LPZ solubility. As shown in Fig. 4a, a slight drop of solubility from 2.96×10^{-4} to 2.01×10^{-4} molar fraction was seen when the temperature was increased from 308 to 328 K at 150 bar [123]. This solubility

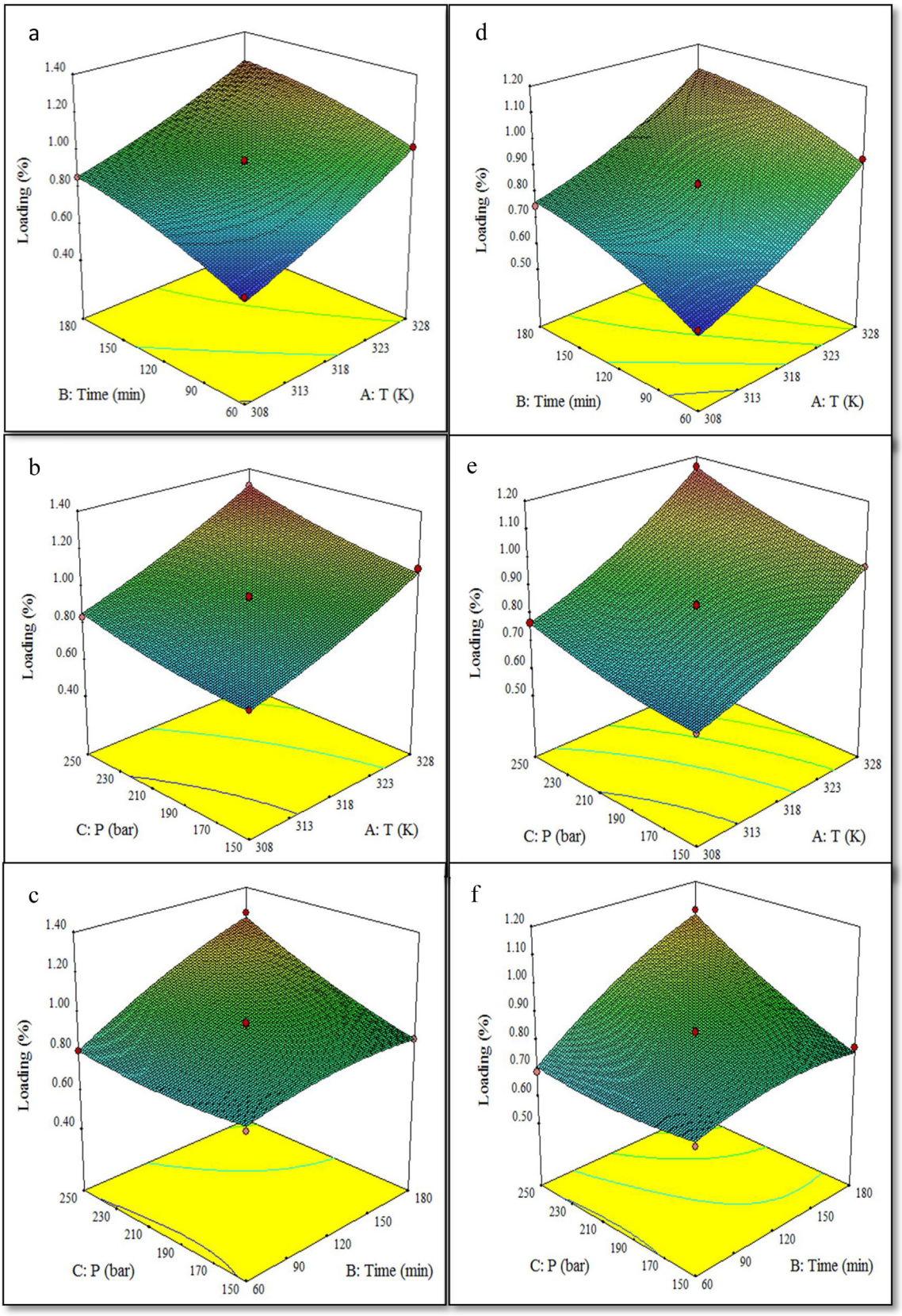

Fig. 3. Response surface plots for the LPZ loading in HPMC (first column): (a) time and temperature, (b) time and pressure and (c) pressure and temperature. Response surface plots for the LPZ loading in PVP (second column): (e) time and temperature (f) pressure and time (g) temperature and pressure.

Table 3
BBD matrix of three independent parameter for impregnation of LPZ/PVP and LPZ/HPMC.

Std. order	Independent variable						Responses			
	Pressure		Temperature		Time		Actual	RSM	Actual	RSM
	X_1	P (bar)	X_2	T(K)	X_3	t(min)	Loading (LPZ/PVP)	Loading (LPZ/PVP)	Loading (LPZ/HPMC)	Loading (LPZ/HPMC)
1	0	200	−1	308	−1	60	0.56	0.54	0.61	0.59
2	0	200	+1	328	−1	60	0.93	0.91	1.02	1.02
3	0	200	−1	308	+1	180	0.75	0.77	0.86	0.86
4	0	200	+1	328	+1	180	1.08	1.10	1.21	1.23
5	−1	150	−1	308	0	120	0.65	0.65	0.72	0.72
6	−1	150	+1	328	0	120	0.97	0.97	1.10	1.08
7	+1	250	−1	308	0	120	0.77	0.77	0.84	0.86
8	+1	250	+1	328	0	120	1.16	1.16	1.30	1.30
9	−1	150	0	318	−1	60	0.70	0.72	0.78	0.81
10	−1	150	0	318	+1	180	0.78	0.76	0.87	0.87
11	+1	250	0	318	−1	60	0.69	0.71	0.81	0.81
12	+1	250	0	318	+1	180	1.09	1.07	1.26	1.23
13	0	200	0	318	0	120	0.83	0.83	0.95	0.94
14	0	200	0	318	0	120	0.83	0.83	0.95	0.94
15	0	200	0	318	0	120	0.81	0.83	0.94	0.94
16	0	200	0	318	0	120	0.84	0.83	0.91	0.94
17	0	200	0	318	0	120	0.83	0.83	0.95	0.94

Table 4
RSM model adequacy analysis of LPZ/PVP.

source	Std.Dev	R-square	Adjusted R-square	Predicted R-square	Sequential P-value	Lack of fitP- value	PRESS
Linear	0.057	0.8987	0.8753	0.7903	<0.0001	0.0018	0.088
2FI	0.039	0.9632	0.9411	0.8209	0.0143	0.0067	0.076
Quadratic	**0.021**	**0.9929**	**0.9837**	**0.9041**	**0.0068**	**0.0548**	**0.040**
Cubic	0.012	0.9989	0.9950		0.0548		

Bold shows that this is the best model.

Table 5
RSM model adequacy analysis of LPZ/HPMC.

Source	Std.Dev	R-square	Adjusted R-square	Predicted R-square	Sequential P-value	Lack of fitP- value	PRESS
Linear	0.062	0.9097	0.8888	0.8133	<0.0001	0.0063	0.10
2FI	0.039	0.9724	0.9558	0.8680	0.0062	0.0310	0.074
Quadratic	**0.025**	**0.9920**	**0.9817**	**0.9017**	**0.0271**	**0.1155**	**0.055**
Cubic	0.017	0.9979	0.9916		0.1155		

Bold shows that this is the best model.

Table 6
RSM model ANOVA analysis of LPZ/PVP.

Source	Sum of squares	df	Mean square	F value	P-Value prob > F	Significance
model	0.42	9	0.047	108.36	<0.0001	Significant
T	0.25	1	0.25	578.36	<0.0001	Significant
time	0.084	1	0.084	195.78	<0.0001	Significant
P	0.047	1	0.047	108.56	<0.0001	Significant
T × time	4.000E−4	1	4.000E−4	0.93	0.3666	Not significant
T × P	1.203E−3	1	1.203E−3	2.80	0.1380	Not significant
P × time	0.026	1	0.026	59.63	0.0001	Significant
T × T	5.622E−3	1	5.622E−3	13.09	0.0085	Significant
time*time	5.492E−3	1	5.492E−3	12.79	0.0090	Significant
P*P	1.954E−3	1	1.954E−3	4.55	0.0703	Not Significant
Residual	3.005E−3	7	4.293E−4			
Lack of fit	2.475E−3	3	8.250E−4	6.23	0.0548	Not significant
Pure Error	5.301E−4	4				
Car Total	0.42	16				

detriment, however, did not affect the LPZ impregnation loading. This implied that the impregnation process could be favored at even low CO_2 solvating powers. This was because of the decrease in the drug affinity with the CO_2 phase that promoted the deviation of the partition coefficient in favor of the polymers. On the other hand, if the drug−CO_2 affinity was lower than that of the drug-polymer, the distribution of the compounds in the supercritical phase was limited, adding to their retention within the matrix [124]. Furthermore, the increase in the swelling with increasing the temperature at constant pressure could be a result of this positive effect. The greater the swelling, the quicker and more complete the diffusion of the impregnation [121]. As can be seen in Table 2, with increasing the temperature at a pressure of 150 bar, the drug loading increased from 0.65 to 0.97% for PVP and from 0.72% to 1.10% for HPMC. From the above discussion, it could be concluded that the drug loading was not only influenced by the solubility of the drug in SC−CO_2, but also by the partition coefficients of the drug in the polymer and the fluid phases.

Table 7
RSM model ANOVA analysis of LPZ/HPMC.

Source	Sum of squares	df	Mean square	F value	P-Value prob > F	Significance
model	0.55	9	0.061	96.12	<0.0001	Significant
T	0.32	1	0.32	499.12	<0.0001	Significant
time	0.12	1	0.12	187.72	<0.0001	Significant
P	0.068	1	1	106.45	<0.0001	Significant
T × time	9.000E−4	1	1	1.41	0.2742	Not significant
T × P	1.681E−3	1	1	2.63	0.1490	Not significant
P × time	0.032	1	1	50.66	0.0002	Significant
T × T	2.226E−3	1	1	3.48	0.1043	Not significant
time*time	5.923E−3	1	1	9.26	0.0188	Significant
P × P	3.299E−3	1	1	5.16	0.0574	Not significant
Residual	4.477E−3	7	6.395E−4			
Lack of fit	3.311E−3	3	1.104E−3	3.79	0.1155	Not significant
Pure error	1.166E−3	4	2.914E−4			
Car total	0.56	16				

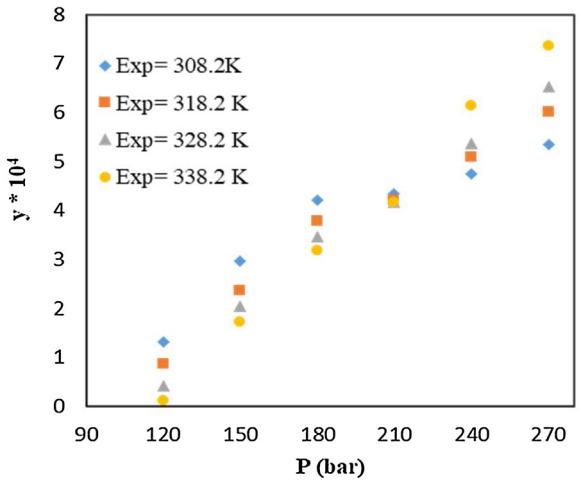

Fig. 4. Experimental LPZ solubility *vs* pressure at various temperatures.

3.2.2. *Effect of pressure*

Considering the effect of pressure, there are two points of view to the subject. Some researchers believed that the solute–CO_2 interactions were intensified beyond the solute-polymer interactions at higher pressures and solvating powers, negatively affecting the amount of loading [10,38,60]. Other researchers [42,71,97,125,126] believed that an increase in pressure tended to increase the swelling and plasticization effects of the polymer; as a result, the solvent could easily transfer the solute into the polymer, thereby enhancing the loading performance while reducing the resistance to drug diffusion. Generally, the influence of these parameters is complex and depends on the different components involved, so that various evolutions could be observed.

The pressure can impose structural impacts on the HPMC and PVP in the course of SC-CO_2 impregnation process. At adequately elevated pressures, CO_2 is soluble in many polymers, leading to concentrations in the range of 10–30 wt.%. This can, in turn, enhance the dissolution of the active ingredient in the SC–CO_2, thereby adding to the swelling of the polymer (*i.e.*, making the polymer amorphous). Also, the absorption of CO_2 by polymers is usually accompanied by a certain degree of swelling (which can be important in biopolymers), which also enhances the impregnation by reducing the resistance to drug diffusion. Pressure can also affect the partition equilibrium of the drug, which basically depends on the balance between the solvating power of CO_2 (which increases with pressure) and particular interactions between the drug and polymer that are presumably important in these systems, due to the presence of polar and H-bonding forming groups. Based on Figs 3b and e, with increasing the pressure from 150 to 250 bar, the loading of the drug on the HPMC and PVP began to increase at a slow rate. Indeed, at a temperature of 308 K with an impregnation time of 120 min, an increase in the pressure from 150 to 250 bar improved the drug loading on both the PVP (from 0.65 to 0.77%) and HPMC (from 0.72 to 0.84%). This indicates the significantly positive effects of pressure on the drug loading when the other operating conditions (*e.g.* temperature and impregnation time) were kept unchanged. This trend was also observed at 328 K; *i.e.* with increasing the pressure from 150 to 250 bar, the LPZ loading increased from 0.97 to 1.16 and from 1.10 to 1.30 for PVP and HPMC, respectively. Examining the loaded amount of drug on the polymer under different operating conditions, it was evident that the best outcomes were observed at a temperature of 328 K. The solubility controls the amount of drug component that can be carried by the fluid phase within the polymeric matrix. Solutes with high solubility in SC-CO_2 can be easily delivered to the impregnation support. The loading of the LPZ could be attributed to the concurrent increase in the solubility of the drug, CO_2 sorption in the matrix and the polymer swelling [55,121]. Similar findings have been reported by other researchers [31,97,125,127]. Bouledjouidja et al. [40] reported similar results for loading foldable commercial intraocular lenses (IOLs). Ngo et al. [125] presented a study on drug impregnation for laser-sintered poly (methyl methacrylate) bio-composites using SC-CO_2. They investigated the effect of pressure in the range of 85–115 bar and figured out that the drug molecules were able to diffuse into the bio-composite at higher pressures. Alessi et al. [97] impregnated piroxicam and nimesulide onto PVP under different sets of conditions. Their experiments at 313 K showed an increase in the drug impregnation with increasing the pressure. In another work, Lauren et al. [58] observed a significant increase in the loading of flax oil onto aerogels upon increasing the pressure from 150 to 300 bar after 4 h of static process.

3.2.3. *Effect of time*

The drug impregnation into the carrier medium is known to be determined by not only the balance among the drug, the polymer, and the SCF, but also the time to reach the equilibrium condition. Based on our previous work, the equilibrium time was about 30 min [123]. Figs. 3c and f demonstrate the effect of impregnation time as it is increased to about 176 min, beyond which time no significant change was seen in the response. However, before the threshold of 176 min, the impregnation time imposed a positive effect on the loading of the drug on the HPMC and PVP. As mentioned previously, various factors such as sorption, the polymer swelling, and diffusivity of the fluid phase within the polymer influence the impregnation loading. Furthermore, the contact time plays an important role not only in the evolution of the diffusion front within the polymer, but also in the quantity of the dissolved drug and the swelling of the polymer by CO_2 sorption. Therefore, it can be concluded that an

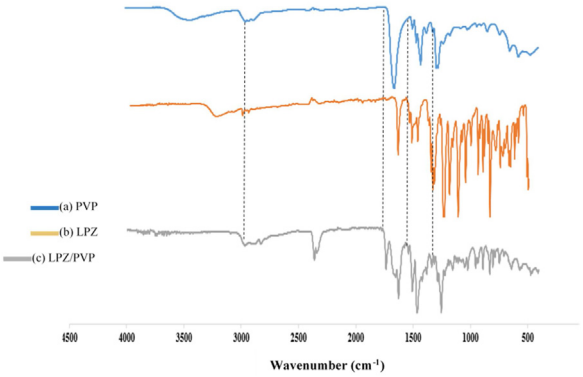

Fig. 5. Comparison of FTIR spectrum for (a) HPMC, (b) LPZ, (c) LPZ/HPMC.

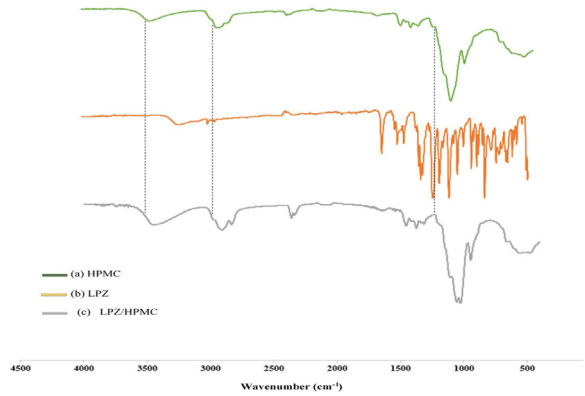

Fig. 6. Comparison of FTIR spectrum for (a) PVP, (b) LPZ, (c) LPZ/PVP.

increase in the impregnation time allows a more in-depth diffusion of the drug facilitated by the improved swelling of the polymer. However, prolonged impregnation times tend to over-enhance the swelling, and the resultant relaxation of the polymer leads to export of the solute from the polymer during the depressurization [43]. Bouledjouidja et al. [40] came with a similar finding. Belizon et al. [38] considered the effect of impregnation time of PET/PP films with methyl gallate (MG) in three different impregnation times, namely 3, 15, and 22 h, at a constant pressure (100 bar) and temperature (35 °C). They observed higher MG loading with increasing the impregnation time. Goni et al. [76] considered the effect of impregnation time of LDPE/sepiolite nanocomposite films with insecticidal terpene ketones in two different impregnation times, namely 2 and 4 h. They noticed higher loading with increasing the impregnation time. Municio et al. [56] reported that the lactulose loading increased from 0.40 to 1.45 upon increasing the impregnation time from 1 to 3 h, confirming the significant effect of the time. Marizza et al. [14,15] identified that the ketoprofen loading can be increased by extending the impregnation time. Testing different impregnation times in the range of 1–4 hr, the best results were achieved with the longest impregnation time, namely 4 h.

3.3. Optimum conditions

In the next step, the considered operating parameters (*i.e.* pressure, temperature and impregnation time) were optimized to reach the maximum loading of LPZ on PVP and HPMC. The optimal values were estimated using the RSM model, with its results compared to the actual data. These parameters were examined in the following ranges:

bar $\leq$ pressure $\leq$ 250 bar

K $\leq$ temperature $\leq$ 328 K

min $\leq$ time $\leq$ 180 min

For both the LPZ/PVP and LPZ/HPMC systems, optimal results (*i.e.* drug loadings of 1.16% and 1.30% for the PVPV and HPMC polymers, respectively) were determined at a pressure of 250 bar, a temperature of 328 K, and an impregnation time of 180 min. For the two systems, the drug loading was found to fall in the following ranges:

0.56% $\leq$ LPZ/PVP $\leq$ 1.16%

0.61% $\leq$ LPZ/HPMC $\leq$ 1.3%

The results of the actual impregnation tests were well in agreement with those of the RSM. Average drug loading was measured at 1.18% $\pm$ 0.03% and 1.34% $\pm$ 0.05% for the PVP and HPMC, respectively.

3.4. Characterization of drug–polymer system

FTIR spectra of the LPZ, PVP, HPMC, LPZ/PVP, and LPZ/HPMC are represented in Figs 5 and 6. The FTIR analysis was performed to identify the drug–polymer interactions for the purpose of analyzing the chemical changes occurred during the SSI. The results showed characteristic peaks indicating the stretching vibration of LPZ (3215.85 cm^{-1}) in relation to the –NH group (disappeared in the solid dispersion) and the $-CH_2$ stretching vibrations at 2983.75 cm^{-1} (attributed to hydrogen bonding between N atoms on the pyridine ring and O atoms on the sulfonyl). The peaks at 1578.44, 1265.11, 1115.38 and 1036.87 cm^{-1} referred to C=N (aromatic ring), CN– (on the pyridine), ether bonding and S=O, respectively. These peaks have been previously identified by Bader et al. and Zhang et al. [1,128].

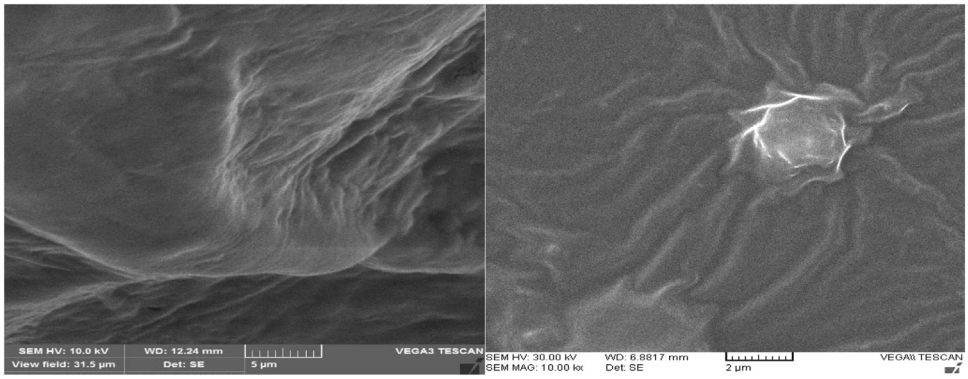

a b

Fig. 7. SEM images of pure of (a) PVP, (b) HPMC.

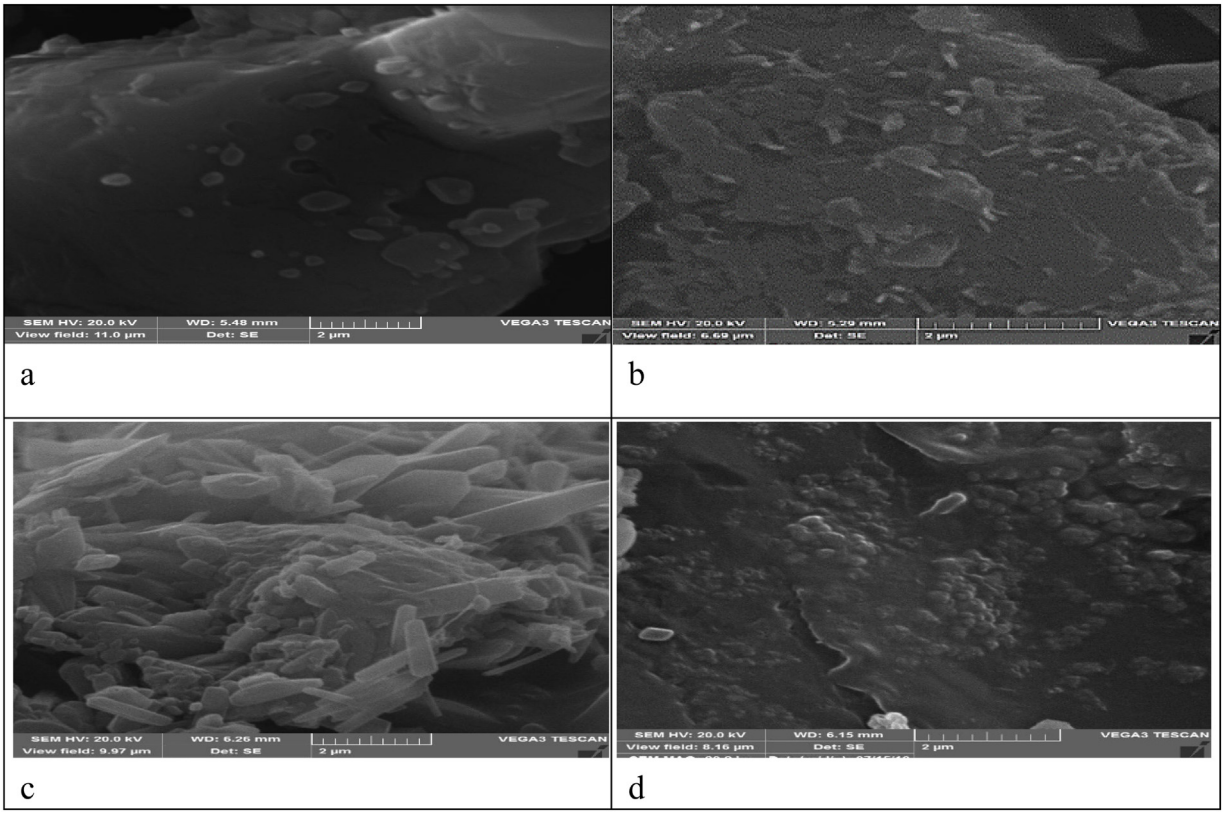

Fig. 8. SEM images of impregnation of LPZ/PVP for: (a) run 1, (b) run 5, (c) run 15, (d) optimum.

The spectrum recorded from the LPZ/PVP system exhibited characteristic absorption peaks at 3441.97, 2948.37 and 1651.53 cm^{-1}. The broad peak seen at 3441.97 cm^{-1} was caused by the presence of water, while the ones at 2948.37 cm^{-1} and 1651.53 cm^{-1} were found to be relevant to the stretching vibrations of the C–H and CO= bonds, respectively. After the impregnation test, the characteristic peak of the water molecules (O—H, ~ 3441.97 cm^{-1}) became thinner. Moreover, upon the impregnation process, the absorption peak at 2948.37 cm^{-1} (attributed to the C–H bond) was intensified while the peak at 1651.53 cm^{-1} underwent a dramatic reduction; the highest absorption peaks were observed in the fingerprint region (900–1100 cm^{-1}) [1].

Analysis of the spectrum recorded from the LPZ/HPMC system showed characteristic peaks in certain ranges. Accordingly, the peaks at 3454.24, 2920.86, and 1634 cm^{-1} belonged to stretching vibrations of the OH, C–H, and CO— bonds for six-membered cyclic rings, respectively. In the range of 1350–1400 cm^{-1}, the peaks corresponding to the C–O–C bond on the cyclic anhydride were observed. The peak in the range of 1300–1200 cm^{-1} was associated with the C—OC— bond on the cyclic epoxide. Finally, the peaks in the ranges of 1100–1000 cm^{-1} and 950–1000 cm^{-1} were attributed to the stretching vibrations of ethereal C—OC— groups and pyranose ring of the HPMC, respectively.

Fig. 5 presents the results of FTIR analysis on the LPZ/HPMC system impregnated by SC-CO_2. The peaks at 3454.24 cm^{-1} and 2920.86 cm^{-1} were associated with –OH stretching vibration and aromatic C–H bonding, respectively, and faded out upon impregnation. High absorption peaks were observed at 1350–1400 cm^{-1} and 1200–1300 cm^{-1} bands, while the ones in the ranges of 1000–1100 and 900–1000 cm^{-1} exhibited lower intensities.

SEM images of the pure polymers are presented in Fig. 7. The SEM images of the impregnation process of the LPZ onto PVP and HPMC show how the drug nanoparticles were incorporated into the polymer matrices (see Figs 8 and 9). The SEM images clearly indicate the drug nanoparticles that were possibly originated upon loading the drugs onto the polymers. As shown in Figs 8d and 9d, the optimum LPZ nanoparticles ended up being well distributed through the PVP or HPMC particles. Results of DLS analysis (Figs 10 and 11) demonstrate the uniform dispersion of the drug particles across the PVP and HPMC. The symmetry on these figures highlights the effectiveness of combining the SC-CO_2 with impregnation method to prevent the drug growth.

The DSC results further shed light on the fact that the PVP and HPMC could prevent the LPZ particle growth, with the polymeric stabilizers controlling the growth of nanoparticles. Figs 12 and 13 show the results of DSC analyses on pure LPZ, pure PVP, pure HPMC, and LPZ/PVP and LPZ/HPMC impregnated systems. The graph of the pure LPZ shows a peak at 180 °C, indicating the melting point of the drug. Also, a sharp endothermic peak was seen immediately after the melting point, which is in agreement with the published data for this drug [1] and the DSC graph for pure lansoprazole analysis by Bader et al. [128]. From the DSC results for the PVP, a broad endotherm ranging from 40 °C to 127 °C was observed, because of the presence of residual moisture in the PVP. Associated with the water loss, this large endotherm over the temperature range 50–130 °C has also been seen in other works [129–132]. Based on the DSC results for the pure HPMC, the endothermic transition starts from 35 and extends to 75 °C, with a broad peak observed in the midway, confirming some of previously reported works [133,134]. Generally, diffusion of SC-CO_2 into a polymer species results in the swelling of the polymer and changes in its mechanical and physical properties. The most important effect of this kind is the reduction of the glass transition temperature (Tg) of a glassy polymer subjected to SC-CO_2, often simply called plasticization. The polymer plasticization results from the ability of CO_2 to interact with the basic sites on the polymer molecules [43]. Sev-

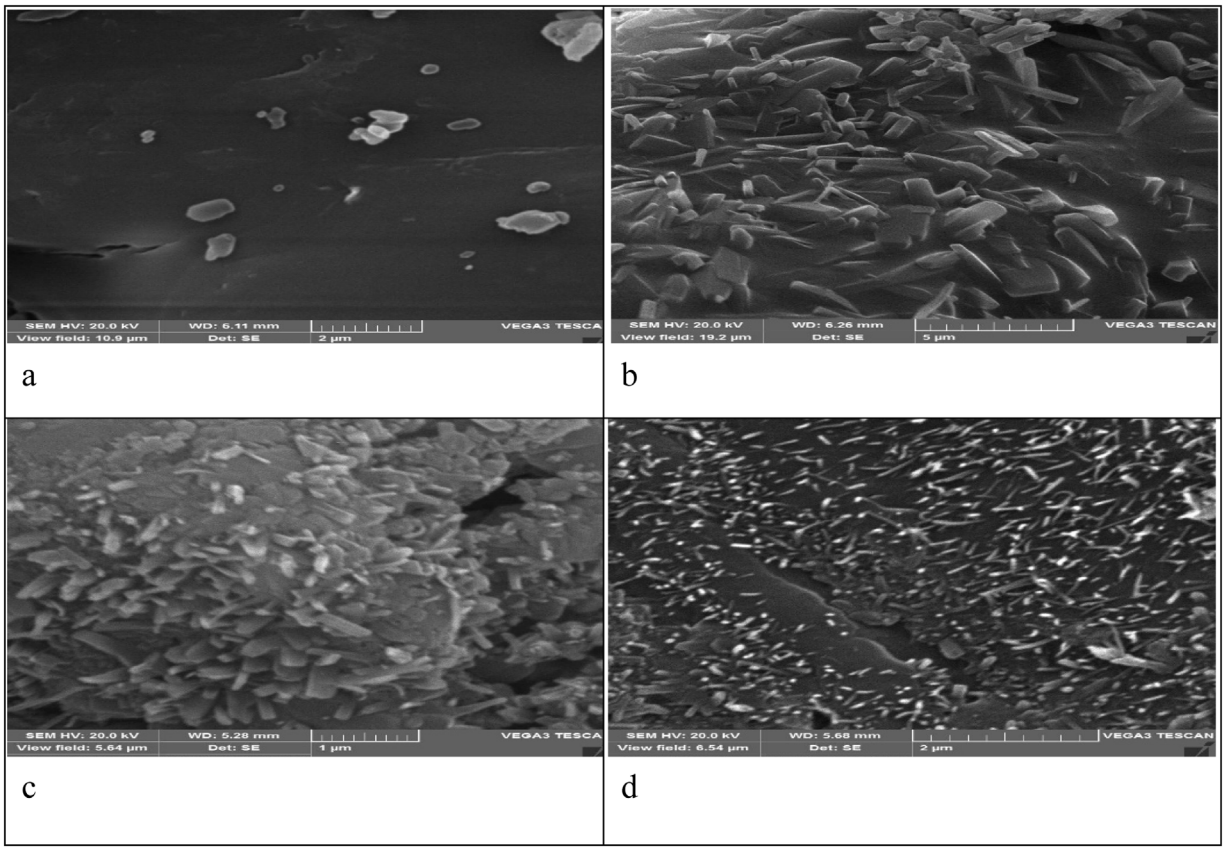

Fig. 9. SEM images of impregnation of LPZ/HPMC for: (a) run1, (b) run 5, (c) run 15, (d) optimum.

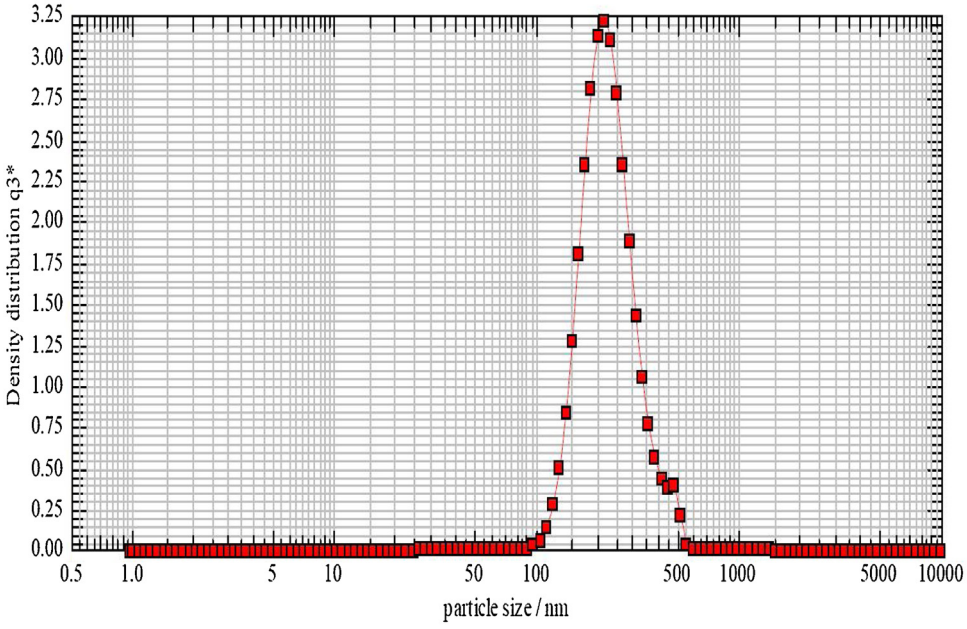

Fig. 10. DLS graphs for optimum condition with impregnation LPZ/PVP.

eral researchers reported that the Tg decreases with increasing the pressure [135–137]. For example in the case of PMMA, the presence of oxygen atoms promotes the interactions with SC-CO_2 and thus reduces the Tg for many glassy polymers [43]. The glass temperature of the PVP has been reportedly measured at around 163 °C (155–160 °C in the present research) [138]. In the case of HPMC, only a tiny change in the baseline is observed around 177 °C. This change corresponds to the polymer Tg, being in agreement with a previously reported value (196 °C) [139,140].

In addition, it was observed that the melting point of LPZ changed after the impregnation test. From the peaks obtained after

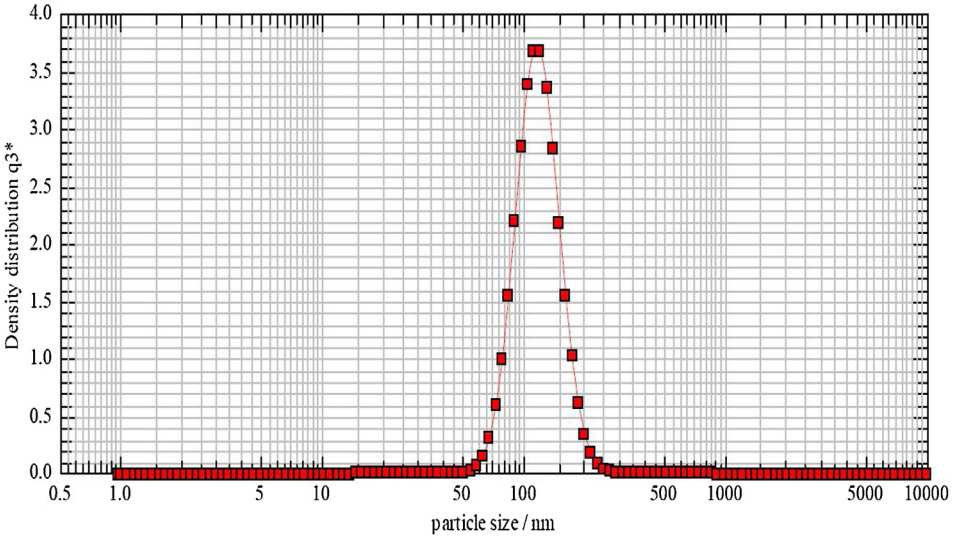

Fig. 11. DLS graphs for optimum condition with impregnation LPZ/HPMC.

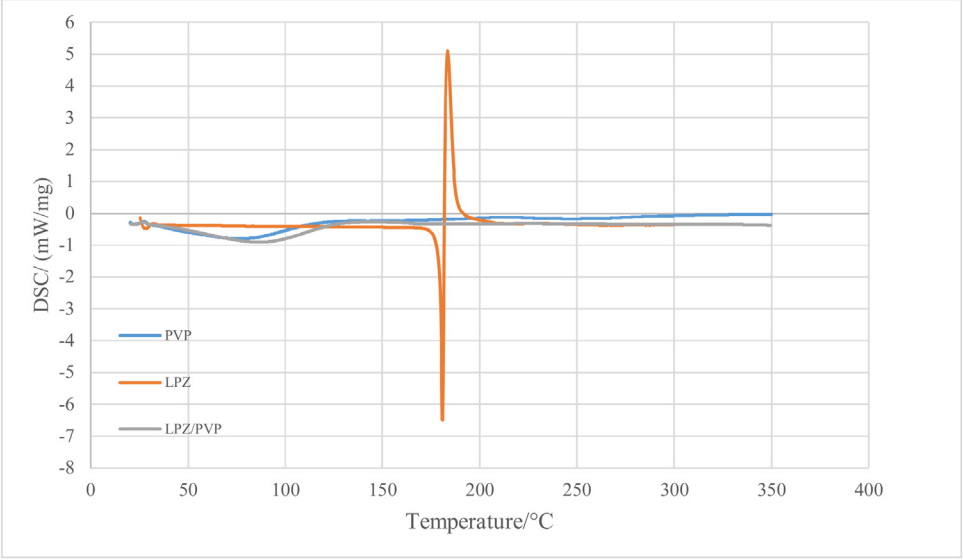

Fig. 12. DSC analysis results of LPZ, PVP before and after the process.

the impregnation tests, the drug was found to be well dispersed through both polymers.

XRD analyses were performed on the LPZ, PVP and HPMC, both before and after the impregnation tests, to evaluate their crystal structure, with the results shown in Figs. 14 and 15. Based on the diffraction pattern obtained from the original LPZ, it was found to be well crystalline with characteristic peaks at 11.331°, 14.160°, 16.835°, 17.454°, 22.262°, 24.906°, and 27.716°. These peaks have been reported for post-impregnation samples in a previous work by Zhang et al. [1], with the degree of crystallinity decreased upon impregnation. The obtained XRD pattern showed no characteristic peak corresponding to the LPZ in the impregnated PVP and HPMC. This was linked to the too small size of the LPZ particles that turn the substance from the crystalline state to amorphous state upon SC-CO_2 impregnation. Furthermore, given that the loading proceeded to no more than 2%, no crystallinity-related peak was observed in the XRD pattern but rather only the amorphous halos and plasticization of the polymers were there. The surface area of the polymers was also measured. Based on the results, the HPMC exhibited a larger surface area (44.83 m^2/g) than the PVP (33.52 m^2/g), possibly due to higher drug loading onto the HPMC. The results of FTIR, DLS, SEM, DSC, and XRD analyses suggested that the drug was only partially miscible in the considered polymers.

4. Conclusion

Supercritical CO_2-assisted impregnation represents a novel approach to the development of green chemistry in the pharmaceutical industry. The impregnation of LPZ onto two different polymers, namely PVP and HPMC, using the supercritical solvent-impregnation method was investigated. After evaluating the operating conditions at lab scale, effects of pressure (150–250 bar), temperature (308–328 K) and impregnation time (60–180 min) on the drug loading were investigated by RSM-BBD through a total of 17 tests. Based on the results, any increase in either of the three parameters led to improvement of the drug loading onto the PVP and HPMC. Indeed, for both of the considered polymers, the optimal results were achieved at a pressure of 250 bar, a temperature of 328 K, and an impregnation time of 176 min. Based on the test results, impregnation loading of LPZ on the PVP and HPMC ranged in

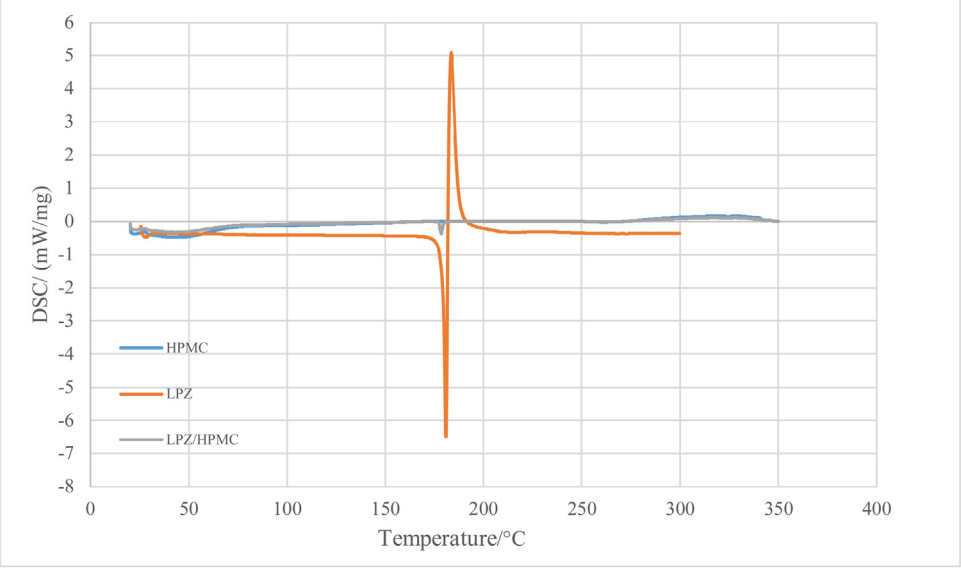

Fig. 13. DSC analysis results of LPZ, HPMC before and after the process.

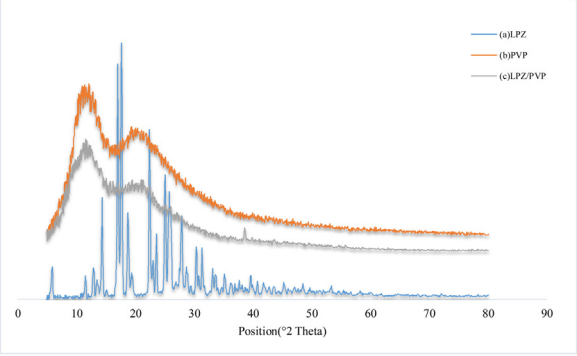

Fig. 14. XRD pattern of LPZ before and after processes (a) LPZ, (b) PVP, (c) LPZ/PVP.

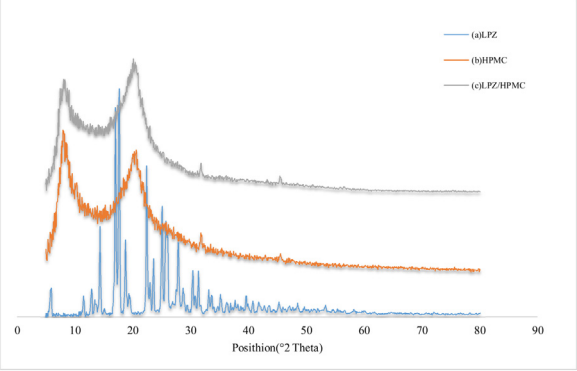

Fig. 15. XRD pattern of LPZ before and after processes: (a) LPZ, (b) HPMC, (c) LPZ/HPMC.

0.56–1.16% and 0.61–1.30%, respectively, with the drug exhibiting higher loadings onto the HPMC rather than PVP under the same laboratory conditions. The samples were further characterized using FTIR, DLS, SEM, DSC, and XRD analyses. The interactions of the PVP and the HPMC with the LPZ were studied by FTIR analysis; the post-impregnation particle size and distribution were characterized by monitoring DLS patterns and SEM studies. Finally, the results showed that the drug was miscible in the polymers.

Declaration of competing interest

The authors declare that they have no known competing financial interests or personal relationships that could have appeared to influence the work reported in this paper.

Acknowledgement

The authors would like to thank the University of Kashan, research deputy, for providing financial support of this project (Grant #Pajoohaneh-1398/4). Moreover, the authors would like to thank the laboratory of supercritical fluids in the University of Kashan for providing experimental facilities.

References

[1] X. Zhang, N. Sun, B. Wu, Y. Lu, T. Guan, W. Wu, Physical characterization of lansoprazole/PVP solid dispersion prepared by fluid-bed coating technique, Powder Technol. 182 (2008) 480–485.
[2] M. Hong, L. Xu, G. Ren, J. Chen, M. Qi, Solubility of lansoprazole in different solvents, Fluid Phase Equilib. 331 (2012) 18–25.
[3] K.C. Lai, S.K. Lam, K.M. Chu, B.C. Wong, W.M. Hui, W.H. Hu, G.K. Lau, W.M. Wong, M.F. Yuen, A.O. Chan, Lansoprazole for the prevention of recurrences of ulcer complications from long-term low-dose aspirin use, N. Engl. J. Med. 346 (2002) 2033–2038.
[4] Y. Fang, G. Wang, R. Zhang, Z. Liu, Z. Liu, X. Wu, D. Cao, Eudragit L/HPMCAS blend enteric-coated lansoprazole pellets: enhanced drug stability and oral bioavailability, AAPS PharmSciTech 15 (2014) 513–521.
[5] C. Wu, L. Sun, J. Sun, Y. Yang, C. Ren, X. Ai, H. Lian, Z. He, Profiling biopharmaceutical deciding properties of absorption of lansoprazole enteric-coated tablets using gastrointestinal simulation technology, Int. J. Pharm. 453 (2013) 300–306.
[6] H. Lai, K. Lin, W. Zhang, Z. Zhang, L. Jie, Y. Wu, Q. He, Development of pH-and enzyme-controlled, colon-targeted, pulsed delivery system of a poorly water-soluble drug: preparation and in vitro evaluation, Drug Dev. Ind. Pharm. 36 (2010) 81–92.
[7] E. Reverchon, R. Adami, Nanomaterials and supercritical fluids, J. Supercrit. Fluids 37 (2006) 1–22.
[8] N. Esfandiari, Production of micro and nano particles of pharmaceutical by supercritical carbon dioxide, J. Supercrit. Fluids 100 (2015) 129–141.
[9] M. Bahrami, S. Ranjbarian, Production of micro-and nano-composite particles by supercritical carbon dioxide, J. Supercrit. Fluids 40 (2007) 263–283.
[10] S. Varona, S. Rodríguez-Rojo, Á. Martín, M.J. Cocero, C.M. Duarte, Supercritical impregnation of lavandin (Lavandula hybrida) essential oil in modified starch, J. Supercrit. Fluids 58 (2011) 313–319.
[11] E. Kiran, Supercritical fluids and polymers – The year in review – 2014, J. Supercrit. Fluids 110 (2016) 126–153.
[12] G. Sodeifian, S.A. Sajadian, Utilization of ultrasonic-assisted RESOLV (US-RESOLV) with polymeric stabilizers for production of amiodarone

hydrochloride nanoparticles: optimization of the process parameters, Chem. Eng. Res. Des. 142 (2019) 268–284.
[13] P. Franco, I. De Marco, Eudragit: a novel carrier for controlled drug delivery in supercritical antisolvent coprecipitation, Polymers 12 (2020) 234.
[14] P. Marizza, S.S. Keller, A. Müllertz, A. Boisen, Polymer-filled microcontainers for oral delivery loaded using supercritical impregnation, J. Control. Release 173 (2014) 1–9.
[15] Y.A. Hussain, C.S. Grant, Ibuprofen impregnation into submicron polymeric films in supercritical carbon dioxide, J. Supercrit. Fluids 71 (2012) 127–135.
[16] G.R. Medeiros, S.R. Ferreira, B.A. Carciofi, High pressure carbon dioxide for impregnation of clove essential oil in LLDPE films, Innov. Food Sci. Emerg. Technol. 41 (2017) 206–215.
[17] M. Chauvet, M. Sauceau, J. Fages, Extrusion assisted by supercritical CO2: a review on its application to biopolymers, J. Supercrit. Fluids 120 (2017) 408–420.
[18] K. Ongkasin, Y. Masmoudi, C.M. Wertheimer, A. Hillenmayer, K.H. Eibl-Lindner, E. Badens, Supercritical fluid technology for the development of innovative ophthalmic medical devices: drug loaded intraocular lenses to mitigate posterior capsule opacification, Eur. J. Pharm. Biopharm. (2020).
[19] M. Perrut, Sterilization and virus inactivation by supercritical fluids (a review), J. Supercrit. Fluids 66 (2012) 359–371.
[20] K. Ongkasin, Y. Masmoudi, C.M. Wertheimer, A. Hillenmayer, K.H. Eibl-Lindner, E. Badens, Supercritical fluid technology for the development of innovative ophthalmic medical devices: drug loaded intraocular lenses to mitigate posterior capsule opacification, Eur. J. Pharm. Biopharm. 149 (2020) 248–256.
[21] M.C. Paisana, K.C. Müllers, M.A. Wahl, J.F. Pinto, Production and stabilization of olanzapine nanoparticles by rapid expansion of supercritical solutions (RESS), J. Supercrit. Fluids 109 (2016) 124–133.
[22] M. PantiŁ, P. Kotnik, Ž. Knez, Z. Novak, High pressure impregnation of vitamin D3 into polysaccharide aerogels using moderate and low temperatures, J. Supercrit. Fluids 118 (2016) 171–177.
[23] D. Bolten, M. Türk, Micronisation of carbamazepine through rapid expansion of supercritical solution (RESS), J. Supercrit. Fluids 62 (2012) 32–40.
[24] P. Trucillo, P. Ferrari, R. Campardelli, E. Reverchon, P. Perego, A supercritical assisted process for the production of amoxicillin loaded liposomes for anti-microbial applications, J. Supercrit. Fluids (2020), 104842.
[25] E. Reverchon, G. Della Porta, Micronization of antibiotics by supercritical assisted atomization, J. Supercrit. Fluids 26 (2003) 243–252.
[26] F.Y. Han, A. Whittaker, S.M. Howdle, A. Naylor, A. Shabir-Ahmed, M.T. Smith, Sustained-release hydromorphone microparticles produced by supercritical fluid polymer encapsulation, J. Pharm. Sci. 108 (2019) 811–814.
[27] L. Lesoin, C. Crampon, O. Boutin, E. Badens, Preparation of liposomes using the supercritical anti-solvent (SAS) process and comparison with a conventional method, J. Supercrit. Fluids 57 (2011) 162–174.
[28] M.J. Cocero, Á. Martín, F. Mattea, S. Varona, Encapsulation and co-precipitation processes with supercritical fluids: fundamentals and applications, J. Supercrit. Fluids 47 (2009) 546–555.
[29] G. Tkalec, M. Pantić, Z. Novak, Ž. Knez, Supercritical impregnation of drugs and supercritical fluid deposition of metals into aerogels, J. Mater. Sci. 50 (2015) 1–12.
[30] P. Franco, E. Pessolano, R. Belvedere, A. Petrella, I. De Marco, Supercritical impregnation of mesoglycan into calcium alginate aerogel for wound healing, J. Supercrit. Fluids 157 (2020), 104711.
[31] A. Rojas, A. Torres, M. José Galotto, A. Guarda, R. Julio, Supercritical impregnation for food applications: a review of the effect of the operational variables on the active compound loading, Crit. Rev. Food Sci. Nutr. (2019) 1–12.
[32] P. Gurikov, I. Smirnova, Amorphization of drugs by adsorptive precipitation from supercritical solutions: a review, J. Supercrit. Fluids 132 (2018) 105–125.
[33] M. Champeau, J.-M. Thomassin, T. Tassaing, C. Jérôme, Drug loading of polymer implants by supercritical CO2 assisted impregnation: a review, J. Control. Release 209 (2015) 248–259.
[34] Z. Ulker, C. Erkey, An advantageous technique to load drugs into aerogels: gas antisolvent crystallization inside the pores, J. Supercrit. Fluids 120 (2017) 310–319.
[35] A. Ubeyitogullari, O.N. Ciftci, Generating phytosterol nanoparticles in nanoporous bioaerogels via supercritical carbon dioxide impregnation: effect of impregnation conditions, J. Food Eng. 207 (2017) 99–107.
[36] M. Pantić, Ž. Knez, Z. Novak, Supercritical impregnation as a feasible technique for entrapment of fat-soluble vitamins into alginate aerogels, J. Non. Solids 432 (2016) 519–526.
[37] S.G. Kazarian, N.H. Brantley, B.L. West, M.F. Vincent, C.A. Eckert, In situ spectroscopy of polymers subjected to supercritical CO2: plasticization and dye impregnation, Appl. Spectrosc. 51 (1997) 491–494.
[38] M. Belizón, M. Fernández-Ponce, L. Casas, C. Mantell, E.M. De La Ossa-Fernández, Supercritical impregnation of antioxidant mango polyphenols into a multilayer PET/PP food-grade film, J. Co2 Util. 25 (2018) 56–67.
[39] L.I. Cabezas, V. Fernández, R. Mazarro, I. Gracia, A. de Lucas, J.F. Rodríguez, Production of biodegradable porous scaffolds impregnated with indomethacin in supercritical CO2, J. Supercrit. Fluids 63 (2012) 155–160.
[40] A. Bouledjouidja, Y. Masmoudi, M. Sergent, V. Trivedi, A. Meniai, E. Badens, Drug loading of foldable commercial intraocular lenses using supercritical impregnation, Int. J. Pharm. 500 (2016) 85–99.
[41] A. Bouledjouidja, Y. Masmoudi, Y. Li, W. He, E. Badens, Supercritical impregnation and optical characterization of loaded foldable intraocular lenses using supercritical fluids, J. Cataract Refract. Surg. 43 (2017) 1343–1349.
[42] A. Bouledjouidja, Y. Masmoudi, M. Sergent, E. Badens, Effect of operational conditions on the supercritical carbon dioxide impregnation of anti-inflammatory and antibiotic drugs in rigid commercial intraocular lenses, J. Supercrit. Fluids 130 (2017) 63–75.
[43] A. Bouledjouidja, Supercritical Fluid Impregnation for the Elaboration of Sustained Drug Delivery, Aix-Marseille Université Sciences de l'environnement, 2016.
[44] V.P. Costa, M.E. Braga, C.M. Duarte, C. Alvarez-Lorenzo, A. Concheiro, M.H. Gil, H.C. de Sousa, Anti-glaucoma drug-loaded contact lenses prepared using supercritical solvent impregnation, J. Supercrit. Fluids 53 (2010) 165–173.
[45] C.C. Bastante, L.C. Cardoso, C.M. Serrano, E.J.M. de la Ossa, Supercritical impregnation of food packaging films to provide antioxidant properties, J. Supercrit. Fluids 128 (2017) 200–207.
[46] C. Tang, Y.-X. Guan, S.-J. Yao, Z.-Q. Zhu, Preparation of ibuprofen-loaded chitosan films for oral mucosal drug delivery using supercritical solution impregnation, Int. J. Pharm. 473 (2014) 434–441.
[47] A. Bouledjouidja, Y. Masmoudi, M. Van Speybroeck, L. Schueller, E. Badens, Impregnation of Fenofibrate on mesoporous silica using supercritical carbon dioxide, Int. J. Pharm. 499 (2016) 1–9.
[48] D. Rusu, C. Cimpoiu, T. Hodişan, The control over the new obtaining procedeum of indomethacin, J. Pharm. Biomed. Anal. 17 (1998) 409–413.
[49] P. Longuemard, M. Jbilou, A.-M. Guyot-Hermann, J.-C. Guyot, Ground and native crystals: comparison of compression capacity and dissolution rate, Int. J. Pharm. 170 (1998) 51–61.
[50] S. Kazarian, G. Martirosyan, Spectroscopy of polymer/drug formulations processed with supercritical fluids: in situ ATR–IR and Raman study of impregnation of ibuprofen into PVP, Int. J. Pharm. 232 (2002) 81–90.
[51] K. Gong, J. Darr, I. Rehman, Supercritical fluid assisted impregnation of indomethacin into chitosan thermosets for controlled release applications, Int. J. Pharm. 315 (2006) 93–98.
[52] L. Manna, M. Banchero, D. Sola, A. Ferri, S. Ronchetti, S. Sicardi, Impregnation of PVP microparticles with ketoprofen in the presence of supercritical CO2, J. Supercrit. Fluids 42 (2007) 378–384.
[53] A.R.C. Duarte, A.L. Simplicio, A. Vega-González, P. Subra-Paternault, P. Coimbra, M. Gil, H.C. de Sousa, C.M. Duarte, Supercritical fluid impregnation of a biocompatible polymer for ophthalmic drug delivery, J. Supercrit. Fluids 42 (2007) 373–377.
[54] F. Belhadj-Ahmed, E. Badens, P. Llewellyn, R. Denoyel, G. Charbit, Impregnation of vitamin E acetate on silica mesoporous phases using supercritical carbon dioxide, J. Supercrit. Fluids 51 (2009) 278–286.
[55] J.-P. Yu, Y.-X. Guan, S.-J. Yao, Z.-Q. Zhu, Preparation of roxithromycin-loaded poly (l-lactic acid) films with supercritical solution impregnation, Ind. Eng. Chem. Res. 50 (2011) 13813–13818.
[56] M. Díez-Municio, A. Montilla, M. Herrero, A. Olano, E. Ibáñez, Supercritical CO2 impregnation of lactulose on chitosan: a comparison between scaffolds and microspheres form, J. Supercrit. Fluids 57 (2011) 73–79.
[57] E.D. Cardona, M. del Pilar Noriega, J.D. Sierra, Oxygen scavengers impregnated in porous activated carbon matrix for food and beverage packaging applications, J. Plast. Film Sheeting 28 (2012) 63–78.
[58] L.M. Comin, F. Temelli, M.D. Saldaña, Barley β-glucan aerogels as a carrier for flax oil via supercritical CO2, J. Food Eng. 111 (2012) 625–631.
[59] L. Cabezas, V. Fernández, R. Mazarro, I. Gracia, A. De Lucas, J. Rodríguez, Production of biodegradable porous scaffolds impregnated with indomethacin in supercritical CO2, J. Supercrit. Fluids 63 (2012) 155–160.
[60] A.P. Almeida, S. Rodríguez-Rojo, A.T. Serra, H. Vila-Real, A.L. Simplicio, I. Delgadilho, S.B. da Costa, L.B. da Costa, I.D. Nogueira, C.M. Duarte, Microencapsulation of oregano essential oil in starch-based materials using supercritical fluid technology, Innov. Food Sci. Emerg. Technol. 20 (2013) 140–145.
[61] A.C. Bierhalz, M.A. da Silva, H.C. de Sousa, M.E. Braga, T.G. Kieckbusch, Influence of natamycin loading methods on the physical characteristics of alginate active films, J. Supercrit. Fluids 76 (2013) 74–82.
[62] A. Torres, J. Romero, A. Macan, A. Guarda, M.J. Galotto, Near critical and supercritical impregnation and kinetic release of thymol in LLDPE films used for food packaging, J. Supercrit. Fluids 85 (2014) 41–48.
[63] A.C. de Souza, A.M. Dias, H.C. Sousa, C.C. Tadini, Impregnation of cinnamaldehyde into cassava starch biocomposite films using supercritical fluid technology for the development of food active packaging, Carbohydr. Polym. 102 (2014) 830–837.
[64] M. Champeau, J.M. Thomassin, T. Tassaing, C. Jerome, Drug loading of sutures by supercritical CO2 impregnation: effect of polymer/drug interactions and thermal transitions, Macromol. Mater. Eng. 300 (2015) 596–610.
[65] C. Potter, Y. Tian, G. Walker, C. McCoy, P. Hornsby, C. Donnelly, D.S. Jones, G.P. Andrews, Novel supercritical carbon dioxide impregnation technique for the production of amorphous solid drug dispersions: a comparison to hot melt extrusion, Mol. Pharm. 12 (2015) 1377–1390.
[66] A. Rojas, D. Cerro, A. Torres, M.J. Galotto, A. Guarda, J. Romero, Supercritical impregnation and kinetic release of 2-nonanone in LLDPE films used for active food packaging, J. Supercrit. Fluids 104 (2015) 76–84.
[67] S. Milovanovic, I. Jankovic-Castvan, J. Ivanovic, I. Zizovic, Effect of starch xero and aerogels preparation on the supercritical CO2 impregnation of thymol, Starch 67 (2015) 174–182.

[68] S. Milovanovic, M. Stamenic, D. Markovic, J. Ivanovic, I. Zizovic, Supercritical impregnation of cellulose acetate with thymol, J. Supercrit. Fluids 97 (2015) 107–115.
[69] M.L. Goñi, N.A. Gañán, M.C. Strumia, R.E. Martini, Eugenol-loaded LLDPE films with antioxidant activity by supercritical carbon dioxide impregnation, J. Supercrit. Fluids 111 (2016) 28–35.
[70] A. Mustapa, A. Martin, L. Sanz-Moral, M. Rueda, M. Cocero, Impregnation of medicinal plant phytochemical compounds into silica and alginate aerogels, J. Supercrit. Fluids 116 (2016) 251–263.
[71] S. Milovanovic, D. Markovic, K. Aksentijevic, D.B. Stojanovic, J. Ivanovic, I. Zizovic, Application of cellulose acetate for controlled release of thymol, Carbohydr. Polym. 147 (2016) 344–353.
[72] A. Ubeyitogullari, O.N. Ciftci, Phytosterol nanoparticles with reduced crystallinity generated using nanoporous starch aerogels, RSC Adv. 6 (2016) 108319–108327.
[73] C.C. Bastante, L.C. Cardoso, C.M. Serrano, E.M. de la Ossa, Supercritical impregnation of food packaging films to provide antioxidant properties, J. Supercrit. Fluids 128 (2017) 200–207.
[74] M.L. Goñi, N.A. Gañán, J.M. Herrera, M.C. Strumia, A.E. Andreatta, R.E. Martini, Supercritical CO2 iof LDPE films with terpene ketones as biopesticides against corn weevil (Sitophilus zeamais), J. Supercrit. Fluids 122 (2017) 18–26.
[75] M.L. Goñi, N.A. Gañán, S.E. Barbosa, M.C. Strumia, R.E. Martini, Supercritical CO2-assisted impregnation of LDPE/sepiolite nanocomposite films with insecticidal terpene ketones: impregnation yield, crystallinity and mechanical properties assessment, J. Supercrit. Fluids 130 (2017) 337–346.
[76] A. Rojas, A. Torres, F. Martínez, L. Salazar, C. Villegas, M.J. Galotto, A. Guarda, J. Romero, Assessment of kinetic release of thymol from LDPE nanocomposites obtained by supercritical impregnation: effect of depressurization rate and nanoclay content, Eur. Polym. J. 93 (2017) 294–306.
[77] A. Torres, E. Ilabaca, A. Rojas, F. Rodríguez, M.J. Galotto, A. Guarda, C. Villegas, J. Romero, Effect of processing conditions on the physical, chemical and transport properties of polylactic acid films containing thymol incorporated by supercritical impregnation, Eur. Polym. J. 89 (2017) 195–210.
[78] N. Alvarado, J. Romero, A. Torres, C.L. de Dicastillo, A. Rojas, M.J. Galotto, A. Guarda, Supercritical impregnation of thymol in poly (lactic acid) filled with electrospun poly (vinyl alcohol)-cellulose nanocrystals nanofibers: development an active food packaging material, J. Food Eng. 217 (2018) 1–10.
[79] J. Sanchez-Sanchez, M. Fernández-Ponce, L. Casas, C. Mantell, E.M. de la Ossa, Impregnation of mango leaf extract into a polyester textile using supercritical carbon dioxide, J. Supercrit. Fluids 128 (2017) 208–217.
[80] L. Sun, P. Han, S. Tang, Preparation of ordered mesoporous alumina Supported-ZnO/NiO nanocomposite using supercritical carbon dioxide impregnation and its photocatalytic performance, ChemNanoMat (2019).
[81] C. López de Dicastillo, C. Villegas, L. Garrido, K. Roa, A. Torres, M. Galotto, A. Rojas, J. Romero, Modifying an active compound's release kinetic using a supercritical impregnation process to incorporate an active agent into pla electrospun mats, Polymers 10 (2018) 479.
[82] D. Medarević, J. Djuriš, S. Ibrić, M. Mitrić, K. Kachrimanis, Optimization of formulation and process parameters for the production of carvedilol nanosuspension by wet media milling, Int. J. Pharm. 540 (2018) 150–161.
[83] R. Kuska, S. Milovanovic, S. Frerich, J. Ivanovic, Thermal analysis of polylactic acid under high CO2 pressure applied in supercritical impregnation and foaming process design, J. Supercrit. Fluids 144 (2019) 71–80.
[84] T.N. Adamović, S.L. Milovanović, D.D. Marković, I.T. Žižović, Impregnation of cellulose acetate films with carvacrol using supercritical carbon ioxide, Tehnika 73 (2018) 19–25.
[85] M.L. Goni, N.A. Ganan, R.E. Martini, A.E. Andreatta, Carvone-loaded LDPE films for active packaging: effect of supercritical CO2-assisted impregnation on loading, mechanical and transport properties of the films, J. Supercrit. Fluids 133 (2018) 278–290.
[86] J.E. Mosquera, M.L. Goñi, R.E. Martini, N.A. Gañán, Supercritical carbon dioxide assisted impregnation of eugenol into polyamide fibers for application as a dental floss, J. Co2 Util. 32 (2019) 259–268.
[87] R. Campardelli, P. Franco, E. Reverchon, I. De Marco, Polycaprolactone/nimesulide patches obtained by a one-step supercritical foaming+ impregnation process, J. Supercrit. Fluids 146 (2019) 47–54.
[88] J.M. Silva, S. Akkache, A.C. Araújo, Y. Masmoudi, R.L. Reis, E. Badens, A.R.C. Duarte, Development of innovative medical devices by dispersing fatty acid eutectic blend on gauzes using supercritical particle generation processes, Mater. Sci. Eng. C 99 (2019) 599–610.
[89] V. Aredo, E.S. Passalacqua, S. Pratavieira, A.L. de Oliveira, Formation of lycopene-loaded hydrolysed collagen particles by supercritical impregnation, LWT 110 (2019) 158–167.
[90] S. Zhan, J. Wang, W. Wang, L. Cui, Q. Zhao, Preparation and in vitro release kinetics of nitrendipine-loaded PLLA–PEG–PLLA microparticles by supercritical solution impregnation process, RSC Adv. 9 (2019) 16167–16175.
[91] R. Monteagudo-Olivan, M.J. Cocero, J. Coronas, S. Rodríguez-Rojo, Supercritical CO_2 encapsulation of bioactive molecules in carboxylate based MOFs, J. Co2 Util. 30 (2019) 38–47.
[92] P. Franco, L. Incarnato, I. De Marco, Supercritical CO2 impregnation of α-tocopherol into PET/PP films for active packaging applications, J. Co2 Util. 34 (2019) 266–273.
[93] V. Zefirov, V. Sizov, M. Kondratenko, I. Elmanovich, S. Abramchuk, V. Sergeyev, M. Gallyamov, Celgard-silica composite membranes with enhanced wettability and tailored pore sizes prepared by supercritical carbon dioxide assisted impregnation with silanes, J. Supercrit. Fluids 150 (2019) 56–64.
[94] C. Villegas, M. Arrieta, A. Rojas, A. Torres, S. Faba, M. Toledo, M. Gutierrez, E. Zavalla, J. Romero, M. Galotto, PLA/organoclay bionanocomposites impregnated with thymol and cinnamaldehyde by supercritical impregnation for active and sustainable food packaging, Compos. Part B Eng. 176 (2019), 107336.
[95] T. Gamse, R. Marr, C. Wolf, K. Lederer, Supercritical CO_2 impregnation of polyethylene components for medical purposes, Hem. Ind. 61 (2007) 229–232.
[96] M.E. Braga, V.P. Costa, M.J. Pereira, P.T. Fiadeiro, A.P.A. Gomes, C.M. Duarte, H.C. de Sousa, Effects of operational conditions on the supercritical solvent impregnation of acetazolamide in Balafilcon A commercial contact lenses, Int. J. Pharm. 420 (2011) 231–243.
[97] P. Alessi, K. Ireneo, C. Angelo, F. Alessia, M. Mariarosa, Polydimethylsiloxanes in supercritical solvent impregnation (SSI) of polymers, J. Supercrit. Fluids 27 (2003) 309–315.
[98] K. Sugiura, S. Ogawa, I. Tabata, T. Hori, Impregnation of tranilast to the poly (lactic acid) fiber with supercritical carbon dioxide and the release behavior of tranilast, Sen'i Gakkaishi 61 (2005) 159–165.
[99] S.-L. Ma, Z.-W. Lu, Y.-T. Wu, Z.-B. Zhang, Partitioning of drug model compounds between poly (lactic acid) s and supercritical CO2 using quartz crystal microbalance as an in situ detector, J. Supercrit. Fluids 54 (2010) 129–136.
[100] A. López-Periago, A. Argemi, J. Andanson, V. Fernandez, C. Garcia-Gonzalez, S. Kazarian, J. Saurina, C. Domingo, Impregnation of a biocompatible polymer aided by supercritical CO_2: evaluation of drug stability and drug–matrix interactions, J. Supercrit. Fluids 48 (2009) 56–63.
[101] Y. Masmoudi, L.B. Azzouk, O. Forzano, J.-M. Andre, E. Badens, Supercritical impregnation of intraocular lenses, J. Supercrit. Fluids 60 (2011) 98–105.
[102] A. Cortesi, P. Alessi, I. Kikic, S. Kirchmayer, F. Vecchione, Supercritical fluids chromatography for impregnation optimization, J. Supercrit. Fluids 19 (2000) 61–68.
[103] S. Yoda, K. Sato, H.T. Oyama, Impregnation of paclitaxel into poly(DL-lactic acid) using high pressure mixture of ethanol and carbon dioxide, RSC Adv. 1 (2011) 156–162.
[104] A.R. Berens, G.S. Huvard, R.W. Korsmeyer, Process for incorporating an additive into a polymer and product produced thereby, in, Google Patents, 1989.
[105] J. Zhang, D.J. Martin, E. Taran, K.J. Thurecht, R.F. Minchin, Effect of supercritical carbon dioxide on the loading and release of model drugs from polyurethane films: comparison with solvent casting, Macromol. Chem. Phys. 215 (2014) 54–64.
[106] F. Lecomte, J. Siepmann, M. Walther, R. MacRae, R. Bodmeier, Blends of enteric and GIT-insoluble polymers used for film coating: physicochemical characterization and drug release patterns, J. Control. Release 89 (2003) 457–471.
[107] F. Lecomte, J. Siepmann, M. Walther, R. MacRae, R. Bodmeier, Polymer blends used for the aqueous coating of solid dosage forms: importance of the type of plasticizer, J. Control. Release 99 (2004) 1–13.
[108] F. Siepmann, J. Siepmann, M. Walther, R. MacRae, R. Bodmeier, Blends of aqueous polymer dispersions used for pellet coating: importance of the particle size, J. Control. Release 105 (2005) 226–239.
[109] F. Siepmann, J. Siepmann, M. Walther, R. MacRae, R. Bodmeier, Polymer blends for controlled release coatings, J. Control. Release 125 (2008) 1–15.
[110] Y. El-Malah, S. Nazzal, Novel use of Eudragit® NE 30D/Eudragit® L 30D-55 blends as functional coating materials in time-delayed drug release applications, Int. J. Pharm. 357 (2008) 219–227.
[111] H. Kranz, S. Gutsche, Evaluation of the drug release patterns and long term stability of aqueous and organic coated pellets by using blends of enteric and gastrointestinal insoluble polymers, Int. J. Pharm. 380 (2009) 112–119.
[112] D. Baş, I.H. Boyacı, Modeling and optimization I: Usability of response surface methodology, J. Food Eng. 78 (2007) 836–845.
[113] K.M. Ara, M. Jowkarderis, F. Raofie, Optimization of supercritical fluid extraction of essential oils and fatty acids from flixweed (Descurainia Sophia L.) seed using response surface methodology and central composite design, J. Food Sci. Technol. 52 (2015) 4450–4458.
[114] D.C. Montgomery, Design and analysis of experiments, in: Design and Analysis of Experiments, 7th ed., John Wiley & Sons, New York, 2009, John Wiley & Sons, New York.
[115] G. Sodeifian, S.A. Sajadian, N.S. Ardestani, Supercritical fluid extraction of omega-3 from Dracocephalum kotschyi seed oil: process optimization and oil properties, J. Supercrit. Fluids 119 (2017) 139–149.
[116] G. Sodeifian, S.A. Sajadian, B. Honarvar, Mathematical modelling for extraction of oil from Dracocephalum kotschyi seeds in supercritical carbon dioxide, Nat. Prod. Res. (2017) 1–9.
[117] M. Ostwal, J.M. Lau, C.J. Orme, F.F. Stewart, J.D. Way, The influence of temperature on the sorption and permeability of CO2 in poly (fluoroalkoxyphosphazene) membranes, J. Membr. Sci. 344 (2009) 199–203.
[118] K. Ghosal, B.D. Freeman, Gas separation using polymer membranes: an overview, Polym. Adv. Technol. 5 (1994) 673–697.

[119] I. Ushiki, Y. Yoshino, S. Hayashi, S.-i. Kihara, S. Takishima, Measurement and modeling of solubilities and diffusion coefficients of carbon dioxide in poly(ethylene-co-acrylic acid), J. Supercrit. Fluids 158 (2020), 104733.
[120] I. Ushiki, S. Hayashi, S.-i. Kihara, S. Takishima, Solubilities and diffusion coefficients of carbon dioxide and nitrogen in poly (methyl methacrylate) at high temperatures and pressures, J. Supercrit. Fluids 152 (2019), 104565.
[121] O. Guney, A. Akgerman, Synthesis of controlled-release products in supercritical medium, AlCHe J. 48 (2002) 856–866.
[122] I. Zizovic, Potential of supercritical solvent impregnation for development of materials with antibacterial properties, Int Arch Med Microbiol 1 (2017).
[123] G. Sodeifian, S.A. Sajadian, R. Derakhsheshpour, Experimental measurement and thermodynamic modeling of Lansoprazole solubility in supercritical carbon dioxide: application of SAFT-VR EoS, Fluid Phase Equilib. 507 (2020), 112422.
[124] J. Sanchez-Sanchez, M. Fernández-Ponce, L. Casas, C. Mantell, E.J. Martínez de la Ossa, Impregnation of mango leaf extract into a polyester textile using supercritical carbon dioxide, J. Supercrit. Fluids 128 (2017) 208–217.
[125] T.T. Ngo, S. Blair, K. Kuwahara, D. Christensen, I. Barrera, M. Domingo, S. Singamneni, Drug impregnation for laser sintered poly (methyl methacrylate) biocomposites using supercritical carbon dioxide, J. Supercrit. Fluids 136 (2018) 29–36.
[126] A.M.A. Dias, M.E.M. Braga, I.J. Seabra, P. Ferreira, M.H. Gil, H.C. de Sousa, Development of natural-based wound dressings impregnated with bioactive compounds and using supercritical carbon dioxide, Int. J. Pharm. 408 (2011) 9–19.
[127] A. Bouledjouidja, Y. Masmoudi, M. Sergent, V. Trivedi, A. Meniai, E. Badens, Drug loading of foldable commercial intraocular lenses using supercritical impregnation, Int. J. Pharm. 500 (2016) 85–99.
[128] B.B. Alsulays, V. Kulkarni, S.M. Alshehri, B.K. Almutairy, E.A. Ashour, J.T. Morott, A.S. Alshetaili, J.-B. Park, R.V. Tiwari, M.A. Repka, Preparation and evaluation of enteric coated tablets of hot-melt extruded lansoprazole, Drug Dev. Ind. Pharm. 43 (2017) 789–796.
[129] P.S. Yadav, V. Kumar, U.P. Singh, H.R. Bhat, B. Mazumder, Physicochemical characterization and in vitro dissolution studies of solid dispersions of ketoprofen with PVP K30 and d-mannitol, J. Saudi Pharm. Soc. 21 (2013) 77–84.
[130] N. Zerrouk, N. Mennini, F. Maestrelli, C. Chemtob, P. Mura, Comparison of the effect of chitosan and polyvinylpyrrolidone on dissolution properties and analgesic effect of naproxen, Eur. J. Pharm. Biopharm. 57 (2004) 93–99.
[131] H. Abdelkader, O.Y. Abdallah, H.S. Salem, Comparison of the effect of tromethamine and polyvinylpyrrolidone on dissolution properties and analgesic effect of nimesulide, AAPS PharmSciTech 8 (2007) E110–E117.
[132] B. Tiţa, A. Fuliaş, G. Bandur, E. Marian, D. Tiţa, Compatibility study between ketoprofen and pharmaceutical excipients used in solid dosage forms, J. Pharm. Biomed. Anal. 56 (2011) 221–227.
[133] Sangappa, T. Demappa, Mahadevaiah, S. Ganesha, S. Divakara, M. Pattabi, R. Somashekar, Physical and thermal properties of 8MeV electron beam irradiated HPMC polymer films, Nucl. Instrum. Methods Phys. Res. B 266 (2008) 3975–3980.
[134] N.S. Rani, J. Sannappa, T. Demappa, Structural, thermal, and electrical studies of sodium iodide (NaI)-doped hydroxypropyl methylcellulose (HPMC) polymer electrolyte films, Ionics 20 (2014) 201–207.
[135] H. Guo, V. Kumar, Solid-state poly (methyl methacrylate)(PMMA) nanofoams. Part I: low-temperature CO2 sorption, diffusion, and the depression in PMMA glass transition, Polymer 57 (2015) 157–163.
[136] Y.P. Handa, P. Kruus, M. O'Neill, High-pressure calorimetric study of plasticization of poly (methyl methacrylate) by methane, ethylene, and carbon dioxide, J. Polym. Sci. Part B: Polym. Phys. 34 (1996) 2635–2639.
[137] D.L. Tomasko, H. Li, D. Liu, X. Han, M.J. Wingert, L.J. Lee, K.W. Koelling, A review of CO2 applications in the processing of polymers, Ind. Eng. Chem. Res. 42 (2003) 6431–6456.
[138] D. Turner, A. Schwartz, The glass transition temperature of poly (N-vinyl pyrrolidone) by differential scanning calorimetry, Polymer 26 (1985) 757–762.
[139] H. McPhillips, D. Craig, P. Royall, V. Hill, Characterisation of the glass transition of HPMC using modulated temperature differential scanning calorimetry, Int. J. Pharm. 180 (1999) 83–90.
[140] A. Gómez-Carracedo, C. Alvarez-Lorenzo, J. Gómez-Amoza, A. Concheiro, Chemical structure and glass transition temperature of non-ionic cellulose ethers, J. Therm. Anal. Calorim. 73 (2003) 587–596.